https://doi.org/10.5194/egusphere-2023-324
Preprint. Discussion started: 6 March 2023

Winter sensitivity of glacial states to orbits and ice sheet heights in CESM1.2

Jonathan R. Buzan[1,2], Emmanuele Russo[1,2,3], Woon Mi Kim[1,2,4], and Christoph C. Raible[1,2]

[1]Climate and Environmental Physics, Physics Institute, University of Bern, Bern, Switzerland
[2]Oeschger Centre for Climate Change Research, University of Bern, Bern, Switzerland
[3]now at Institute for Atmospheric and Climate Science, ETH Zurich, Zürich, Switzerland
[4]now at Climate and Global Dynamics, National Center for Atmospheric Research, Boulder CO, USA

Correspondence: Jonathan R. Buzan (jonathan.buzan@unibe.ch)

Abstract. The changing climate system between icehouse and greenhouse states during the Quaternary Period were dramatic, yet the magnitude of these changes are still uncertain due to unconstrained ice sheets and a lack of transition mechanisms. In this study, we investigate the individual and combined impact of ice sheet heights, orbital configurations, and greenhouse gas changes for a range of Quaternary climate states to assess the linearity or non-linearity of the climate system's response. To this end, we conduct two sets of sensitivity experiments: a series on the Preindustrial (PI) climate and experiments on Quaternary glacial states. First, modifying the PI conditions with respect to orbit, Greenland ice sheet height, and greenhouse gasses, we find that the climate system's response to the individual factors do not superimpose on the combined response of the climate system. Thus, already under PI conditions the climate system responds in a non-linear fashion. Second, our results on Quaternary glacial states show that changing ice sheet height is the primary cause of changes in climate systems, regardless of orbit. But the subtle regional effects that orbit has are not always explained by ice sheet height changes. As for the PI simulations we find a strong, non-linear behavior in combined orbital-ice sheet height effect, where the response of the atmospheric circulation plays an important role. Therefore, orbit, ice sheets, and greenhouse gasses evolve through time by specific pathways and imply a theoretical constraint on the real climate state. As the spatial and temporal resolution of the Quaternary proxy data improves, combined with these modeled climates, we expect to generate substantial constraints on the number of realistic Quaternary climate states.

1 Introduction

The climate system of the Quaternary Period (roughly the past 1.8 million years) shows a large range of variability in its icehouse and greenhouse states. These variations result from non-linear climate responses. But the magnitude of these responses is not well constrained, as differing estimates show (Tierney et al., 2020b; Annan et al., 2022), and the underlying mechanisms are not fully understood. Another source of uncertainty arise from unconstrained ice sheet configurations during the Quater-

https://doi.org/10.5194/egusphere-2023-324
Preprint. Discussion started: 6 March 2023

nary Period, as recent reconstructions demonstrate (Peltier et al., 2015; Batchelor et al., 2019). However, although not fully constrained, the estimated magnitudes of change between the Last Glacial Maximum (LGM) and today is in the range of potential future climates, making the LGM a focal period for Paleo Modelling Intercomparison Projects (PMIP; e.g., Abe-Ouchi et al., 2015; Kageyama et al., 2017, 2018). Recent research used the LGM-to-present-day climate response derived from paleo proxy data from PMIP archives to constrain a climate model in order to increase the reliability of projections about future climate changes (Tierney et al., 2020b; Zhu et al., 2022). These results improve the confidence of climate model projections, but with the uncertainties around Quaternary climates, exploring the sensitivity of glacial states to orbit and ice sheets will further characterize these climate states. The purpose of this study is to understand the sensitivity of the climate system to changes in ice sheet heights, Quaternary orbits, greenhouse gases, and their combinations, increasing the model's overall reliability. We use two sets of sensitivity experiments under the Preindustrial and Quaternary glacial states, and by performing sensitivity simulations where only one factor and combination of factors are changed, we disentangle individual causal relationships, as well as non-linear behavior.

1.1 Paleoclimate reconstructions and modeling

One method to assess climatic variability in the Quaternary Period are proxy reconstructions, based mainly on archived ice and sediment cores (Waelbroeck et al., 2009; EPICA Community Members, 2004; Lambert et al., 2008), but the temporal and spatial coverage is rather sparse for the entire period. While the LGM has substantially more data availability as compared to the early Quaternary (Bartlein et al., 2011; Cleator et al., 2020), there is substantial disagreement between recent reconstructions of the temperature amplitude between the LGM and present day. For example, Tierney et al. (2020b) gives an estimate of -6.5°C to -5.7°C, whereas newer reconstructions suggest a range of -4.8°C to -3.2°C (Annan et al., 2022). One reason for this discrepancy lies in the reconstruction methods used: isotopes as a tracer constraining a simulation (Tierney et al., 2020b) versus the multi-model ensemble Kalman filtering (Evensen, 2003; Annan et al., 2022). But because temperature proxies are heavily dependent on their individual calibrations, they can produce substantial errors in their expected temperature values, as the above studies show.

Given the proxy uncertainty and sparseness in time and space for the Quaternary Period, climate modelling is a promising way to fill in gaps within the data. However, only Earth models of intermediate complexity (EMIC; Claussen et al., 2002; Stocker et al., 1992; Willeit et al., 2022) can presently simulate glacial-interglacial cycles while still capturing the global scale of climate variability. But within EMICs, important processes are heavily simplified, such as when the atmospheric component is described statistically or with a simple energy balance model. More complex models, such as Earth System Models (ESM), overcome most of these simplifications, but are limited to transient simulations of a few thousand years due to their high computational costs (Abe-Ouchi et al., 2015; Hofer et al., 2012a, b; Merz et al., 2013, 2015; Otto-Bliesner et al., 2017; Zhu et al., 2017; Kageyama et al., 2017, 2018). Complex ESMs can be simplified however— making orbits change 5 times faster and using a coarse resolution ($\sim$3.75° $\times$ 3.75°) — to run for more than 100,000 years, rather than 1000s, but again have high computational costs (Timmermann et al., 2022). Instead of simplifying ESMs to run continuous time series, time slices are used. Specifically, a battery of different ESMs all use the same LGM boundary conditions are in model intercomparison

https://doi.org/10.5194/egusphere-2023-324
Preprint. Discussion started: 6 March 2023

projects (PMIP; Abe-Ouchi et al., 2015; Kageyama et al., 2017, 2018). These intercomparison projects mainly assess models' ability to simulate the last glacial cycle.

There are many different ESMs available, but due to recent advancements in reproducing the LGM (Tierney et al., 2020b), we focus on the ESM used in this study, the Community Earth System Model version 1 (CESM1; Hurrell et al., 2013). Specifically, we focus on studies performed within the CESM model family, first showing the history and versatility of the model family, then highlighting their results. The past decades produced a series of Quaternary climate sensitivity simulations using CESM and its predecessors, the Community Climate System Model, CCSM1, CCSM3, and CCSM4 (Zhu et al., 2017; Tierney et al., 2020a, b; Windler et al., 2020; Zhu et al., 2021, 2022). Over the years various techniques and shortcuts reduced the computational time it took to reach a climate equilibrium. For example, CCSM1 LGM was initialized with a modern ocean and used an acceleration technique to speed up the time it takes for the ocean to reach equilibrium (Bryan, 1984; Shin et al., 2003). That CCSM1 ocean equilibrium then initialized the fully-coupled CCSM3 model simulation that was executed for 1,862 years (Brandefelt and Otto-Bliesner, 2009). This simulation became the basis of a series of sensitivity experiments, focusing primarily on atmospheric simulations from the Community Atmospheric Model (e.g. CAM3, CAM4, etc.). Some experiments used CAM3 with a thermodynamic ocean (known as slab ocean) derived from the previously mentioned simulation to make boundary condition changes and evaluate Marine Isotopic Stage (MIS) 4 and 5b, the Interglacial, and the LGM (Löfverström et al., 2014; Liakka et al., 2016; Liakka and Löfverström, 2018; Löfverström et al., 2016). Other research groups used fully coupled CCSM3 simulations to derive fixed sea surface temperature (SST) simulations, driving CAM4 simulations with sensitivity changes to ice sheet heights and MIS4 orbits (Hofer et al., 2012a, b; Merz et al., 2015). CCSM4 had its own spin up routine, described in detail later. All of these model techniques may have introduced errors into the resulting climate state but were necessary to reduce computational expenses. For example, the simulated global mean surface temperatures from the fully coupled CCSM1 simulation were colder in the tropics as compared to the CLIMAP datasets (CLIMAP, 1981), which were state-of-the-art for the time (Shin et al., 2003). The CCSM3 global mean surface temperature change was -6.5°C from the Preindustrial (Brandefelt and Otto-Bliesner, 2009), while the CCSM4 global mean land surface temperature change was -6.5°C from the Preindustrial and -2.7°C for the ocean (Brady et al., 2013).

The previously mentioned sensitivity experiments highlighted a variety of atmospheric responses to the changing ice sheets. An increasing ice sheet height leads to a southward displacement of the jet stream (Hofer et al., 2012a, b; Merz et al., 2015). The southward displacement of jet stream then leads to strong changes in Northern Hemisphere precipitation during the winter and minimal changes in the summer (Hofer et al., 2012a). Additionally, the ice sheet changes the atmospheric structure. Winter glacial atmospheric circulation types are dominated by patterns with an east-west pressure gradient over Europe, which contrasts with the predominantly zonal patterns for the recent past (Hofer et al., 2012b).

More recent studies focus on the dynamic changes that occur from changing ice sheets. Stationary and transient wave interaction explains the southern shift of the jet stream over the North Atlantic and the associated changes over Europe (Merz et al., 2015), as well as the planetary wave breaking and reflection results from increasing the ice sheet height (Löfverström et al., 2014; Löfverström et al., 2016). This, in turn, may mean that the North American ice sheet might have largely controlled the size of the Fennoscandinavian ice sheet (Liakka et al., 2016). Finally, there are also teleconnection responses to raising the

https://doi.org/10.5194/egusphere-2023-324
Preprint. Discussion started: 6 March 2023

ice sheet; when the ice sheet is increased, Arctic temperatures also increase $\sim 1.5°$C per km of ice sheet height (Liakka and Löfverström, 2018).

But none of these sensitivity experiments were conducted with fully coupled ESMs, making it unclear how much the estimated changes between glacial states is dependent on ocean-atmospheric coupled responses. To reduce this uncertainty, we perform all sensitivity simulations with a fully coupled model, rather than combining previous versions of a CESM equilibrium simulation to drive a fixed SST or slab ocean. In a first set of experiments, CESM1 quantifies the impacts of ice height, orbit, and greenhouse gas changes by considering each component incrementally, showing that they combine through non-linear impacts, with the PI states serving as a reference. In the second set, we use 4 different glacial ice sheet heights and 4 glacial maximum orbital states (LGM, and Marine Isotopic Stages 4, 6, and 8), for a total of 16 sensitivity experiments. These orbits are known glacial maximal states, and the 4 ice sheet heights are within the range of estimated ice volumes. We analyze these simulations in two ways: one, the explicit effect of changing orbits while holding the ice sheet constant and two, the explicit effect of changing ice sheet heights while holding the orbit constant. In both sets, comparing all these simulations with each other enables us to detect the climate system's linear and non-linear responses to the different sensitivities. The study is structured as follows. In Section 2, we introduce the experimental setting of sensitivity tests. Following the experimental design section, we present the sensitivity of the climate system under Preindustrial climate conditions in Section 3.1. In Section 3.2 we evaluate the glacial simulation for the LGM, and results of the Quaternary simulations are presented in Sections 3.3 and 3.4. Finally, we discuss the results in Section 4 and present our concluding remarks in Section 5.

2 Model and experimental design

2.1 Model description

In this study, we employ the CESM (version 1.2.2; Hurrell et al., 2013), developed at the National Center for Atmospheric Research (NCAR). CESM consists of fully-coupled component models representing different climate sub-systems: the Community Atmospheric Model (CAM5), the Parallel Ocean Program (POP2), the Community Sea Ice Model (CICE), and the Community Land Model (CLM4). A detailed description of these individual component models are documented in Danabasoglu et al. (2012) and Hurrell et al. (2013), and the differences between the previous model version, CCSM4, in Meehl et al. (2013). For the atmosphere and land components, we use a finite volume horizontal resolution of $1.9° \times 2.5°$ (latitude $\times$ longitude), and for the ocean and sea ice model components, the horizontal resolution is the nominal $1°$ displaced pole Greenland grid. The current version is also published with LGM studies Zhu et al. (2017); Tierney et al. (2020b), and various versions of CESM were widely used in paleo-simulations (e.g., Otto-Bliesner et al., 2013; Hofer et al., 2012b, a; Merz et al., 2013, 2014b, a, 2015, 2016).

https://doi.org/10.5194/egusphere-2023-324
Preprint. Discussion started: 6 March 2023

2.2 Experimental design

The experimental design focuses on capturing the variability of glacial states. Sensitivity simulations, through orbital and ice sheet height changes, are applied to both the Preindustrial (PI) and Last Glacial Maximum (LGM) climate states (Zhu et al., 2017).

The reference experiment is a PI control simulation, using perpetual 1850 CE conditions. The simulation is scientifically validated by NCAR and designed for comparing climate change in paleo and future climate. The NCAR PI control is a reference point for the differences between a pre-anthropogenic climate (interglacial state) and the glacial states. We use restart files from an existing CAM5 LGM simulation provided by NCAR (Zhu et al., 2017), achieving equilibrium through acceleration techniques (Brady et al., 2013) similar to ones mentioned for CCSM1 through CCSM3 above. First, the CCSM4 PI was executed for 600 years with the LGM CO_2 value. Second, the simulation was extended 1,000 years while the ocean salinity was changed along with the PMIP3 protocol changes (Morrill et al., 2013) for bathymetry, land surface, and the introduction of ice sheets. This ocean state was used as the initial condition for CESM1 (Zhu et al., 2017) following PMIP4 protocols (Williams et al., 2020; Kageyama et al., 2017, 2018), which ran for 500 years, bringing the total to 2,100 years. After receiving these restart files from NCAR, we extended the simulation for 100 years to check for instabilities. Tests showed that the simulation is in quasi equilibrium (defined as the absolute radiation imbalance <0.32 W/m^2).

The first set of sensitivity experiments determines the linear additive or non-linear properties of PI climate changes through a series of 7 sensitivity experiments (1850 CE). Five experiments modify the PI orbit (Table 1), greenhouse gases (Table 2), and the Greenland ice sheet height (Table 3 and Fig. 1). Within the 5 experiments, the first 3 simulations are single changes: the Last Glacial Maximum greenhouse gases (PI_{GH}), Last Glacial Maximum orbit (PI_{ORB}), and Greenland ice sheet height at 125% (PI_{GL}). The last 2 simulations combine changes: the Last Glacial Maximum orbit and Greenland ice sheet height at 125% ($PI_{ORB,GL}$), and the Last Glacial Maximum orbit and greenhouse gases with Greenland ice sheet height at 125% ($PI_{ORB,GL,GH}$). The last 2 simulations also approximate the PI land cover for the Late Holocene (LH) and Representative Concentration Pathway 8.5 (RCP85). The LH simulation uses an orbit configuration and greenhouse gases from 1500 BCE and a land cover fixed at the year 850 CE. The RCP85 simulation is a transient simulation by design and the orbit configuration and land cover are fixed at the year 1990, with only greenhouse gases changing. From the RCP85 simulation, we extract the last 20 years of the 21st century to evaluate climate properties. If the climate responds linearly to the boundary changes, the simulations with single changes summed together should equal the simulations with multiple changes.

The second set of experiments assesses the influence of orbital forcing during glacial times. We extend an existing 2,100 year LGM simulation for another 100 years (as mentioned before), which is in quasi equilibrium (Zhu et al., 2017). This simulation uses the LGM orbital parameters given in Table 1, the greenhouse gas concentrations and land use changes suggested by Paleoclimate Modelling Intercomparison Project version 4 (PMIP4) protocol (Kageyama et al., 2017), and the ice sheet reconstructions from the ICE-6G (Peltier et al., 2015). While there are additional ice sheet configurations available (Dalton et al., 2022; Batchelor et al., 2019), we use the established framework for comparison with the latest research from the NCAR general circulation model. This extended LGM simulation is a starting point for the sensitivity simulations with different orbital

https://doi.org/10.5194/egusphere-2023-324
Preprint. Discussion started: 6 March 2023

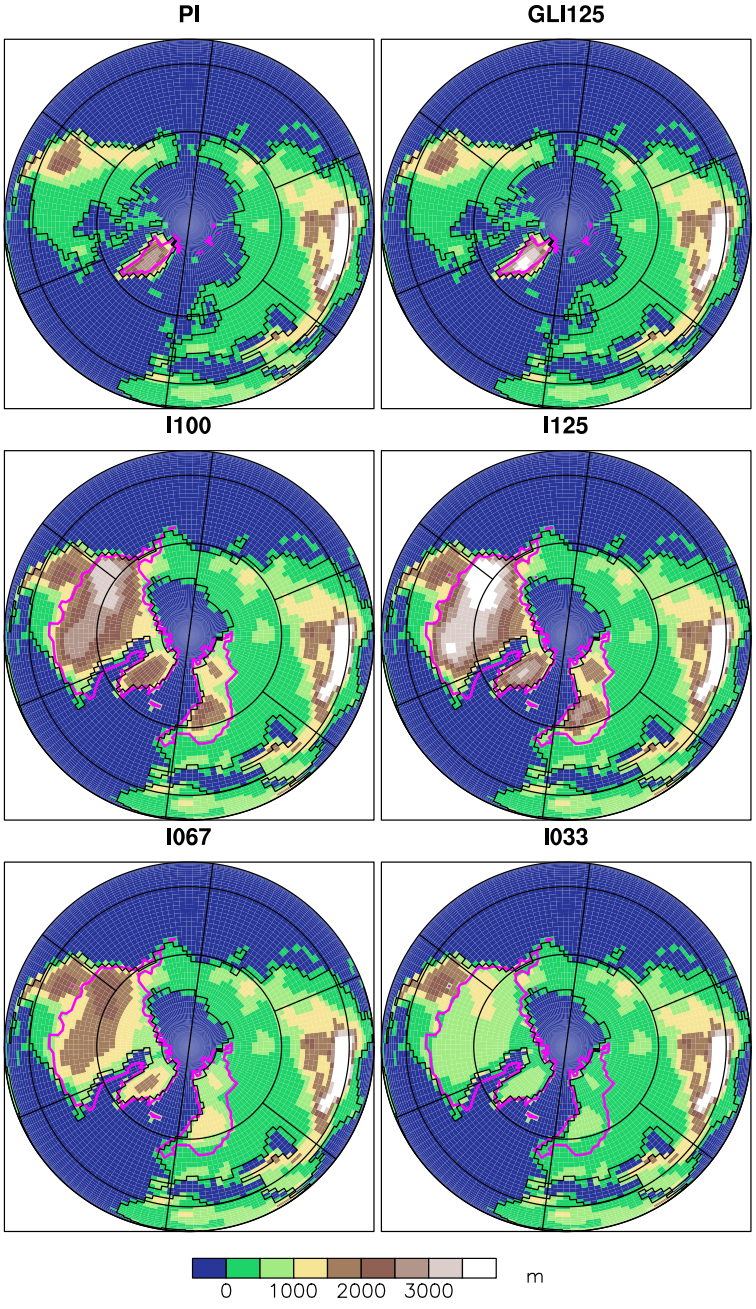

Figure 1. Ice sheet configurations (magenta lines) and orography including the ice sheets (m a.s.l.) for PI, Greenland at 125% (GLI125), and implementation of Peltier et al. (2015) at 100% (I100), 125% (I125), 67% (I067), and 33% (I033).

configurations. We branch three simulations with orbital configurations of MIS4, MIS6, and MIS8 (Table 1) from the LGM simulations and run the simulations to a quasi-equilibrium (again, defined as absolute radiation imbalance < 0.32 W/m^2). The

https://doi.org/10.5194/egusphere-2023-324
Preprint. Discussion started: 6 March 2023

Table 1. Overview of the orbital forcing parameter values applied in the different simulations for the Common Era (CE) and the Before Common Era (BCE). The different periods are Preindustrial (PI), Last Glacial Maximum (LGM), and Marine Isotope Stages (MIS4, MIS6, and MIS8).

Period	Year	Obliquity	Eccentricity	Precession
PI	1850 CE	23.453°	0.016764	280.327°
RCP85	1990 CE	23.4411°	0.016708	282.724°
LH	1500 BCE	23.8709°	0.017969	223.499°
LGM	19050 BCE	22.9490°	0.018994	294.425°
MIS4	60050 BCE	22.9235°	0.018871	61.580°
MIS6	181000 BCE	22.9845°	0.040383	340.416°
MIS8	289000 BCE	23.9235°	0.030817	104.930°

Table 2. Overview of greenhouse gas concentrations for each simulation. The RCP8.5 forcing is transient; here, we show the time means over the last 20 years of the 21st century.

Period	CO_2 (ppm)	CH_4 (ppb)	N_2O (ppb)	F_{11} (ppt)	F_{12} (ppt)
PI	284.7	791.6	275.68	12.48	–
RCP85	781.9724	3518.456	411.1797	954.9954	221.6178
LH	274.0594	261.0723	588.0466	33.432	–
LGM	190	375	200	–	–
MIS4	190	375	200	–	–
MIS8	190	375	200	–	–
MIS6	190	375	200	–	–

other external forcing, such as greenhouse gas concentrations, land use, and, in particular, the ice sheets, remain unchanged in these sensitivity simulations. To illustrate this, the simulations are labeled with respect to their orbital configurations (LGM, MIS4, MIS6, and MIS8) and the ice sheet height (I100, i.e., 100% LGM ice sheet height) as the index: LGM_{I100}, $MIS4_{I100}$, $MIS6_{I100}$, and $MIS8_{I100}$ (Table 1).

160 The third set of experiments investigates the impact of different ice sheet heights during glacial times on climate variability. Given the high uncertainty of ice sheet reconstructions (Peltier et al., 2015; Abe-Ouchi et al., 2015; Ganopolski and Brovkin, 2017; Batchelor et al., 2019), we modify the ice sheet heights to 125%, 67%, and 33% of the LGM ice sheet height (using the index I125, I067, and I033 respectively), which roughly covers the physical range of ice sheet heights over the Quaternary period (Fig. 1). The spatial extent of ice sheets in different glacial maximum states are relatively static, as shown in CLIMBER-
165 2 ice sheet simulations (Ganopolski and Brovkin, 2017). Thus, the height of the Northern Hemisphere ice sheets are only scaled by the three factors (125%, 67%, and 33%). To save computational resources, these sensitivity simulations are branched from the corresponding orbital sensitivity simulations with 100% LGM ice sheet height, resulting in twelve simulations: LGM_{I033},

https://doi.org/10.5194/egusphere-2023-324
Preprint. Discussion started: 6 March 2023

Table 3. Overview of the ice sheet configurations for all simulations: the PI ice sheet (Modern), PI with Greenland Ice Sheet at 125% (GL), LGM ice sheet at 125%, 100%, 67%, and 33% (I125, I100, I067, I033; Peltier et al., 2015).

Period	Modern	GL	I125	I100	I067	I033
PI	√	–	–	–	–	–
PI_{GH}	√	–	–	–	–	–
PI_{ORB}	√	–	–	–	–	–
PI_{GL}	–	√	–	–	–	–
$PI_{ORB,GL}$	–	√	–	–	–	–
$PI_{ORB,GL,GH}$	–	√	–	–	–	–
RCP85	√	–	–	–	–	–
LH	√	–	–	–	–	–
LGM	–	–	√	√	√	√
MIS4	–	–	√	√	√	√
MIS6	–	–	√	√	√	√
MIS8	–	–	√	√	√	√

LGM_{I067}, LGM_{I125}, $MIS4_{I033}$, $MIS4_{I067}$, $MIS4_{I125}$, $MIS6_{I033}$, $MIS6_{I067}$, $MIS6_{I125}$, $MIS8_{I033}$, $MIS8_{I067}$, and $MIS8_{I125}$ (Table 3). Again, the simulations are run in a quasi-equilibrium state with the absolute radiation imbalance of < 0.32 W/m^2.

In summary, we conducted 24 simulations: PI control, 7 PI sensitivities, and 4 each of LGM, MIS4, MIS6, and MIS8. Each simulation runs for up to 400 years until a quasi-equilibrium state is reached (excluding the RCP85 simulation). For analysis, we only used the last 20 years of simulations to evaluate the climate state. Note that the matrix structure of the sensitivity simulations enables us to assess the individual sensitivities because of orbital forcing and ice sheet height, as well as their combined effects.

3 Results

The main purpose of the study is to assess the changes in the LGM sensitivities to orbit and ice sheet heights. However, we first need to demonstrate how a well described climate, the PI, responds to changes. Following that, we then evaluate the LGM_{I100} as compared to proxy data, demonstrating the ability of CESM to capture the glacial environment. Finally, we show the LGM sensitivities in terms of orbits and ice sheet height changes. All of the analysis is conducted through the lens of boreal winter (December to February) in 20 year climatologies, as the atmospheric circulation is intensified during winter season. We focus on temperature and precipitation, looking at how they propagate throughout the atmosphere using simplified stationary wave analysis through geopotential height, removing the zonal means, a measure for planetary wave structures. Temperature and precipitation are critical components for the glacial-interglacial climates and atmospheric circulation and can provide a hint as to how they change non-linearly.

https://doi.org/10.5194/egusphere-2023-324
Preprint. Discussion started: 6 March 2023

3.1 Sensitivity of Preindustrial climate system to 7 Earth system boundary changes

To better constrain the climate system's linear and nonlinear responses to external forcings, we start the analysis under PI conditions, modifying the PI orbit, greenhouse gases, the Greenland ice sheet height, in addition to various combinations of these factors. If we can extract robust predictive quantities, a well-informed statistical model can produce past and future projections.

First, we compare the sensitivity simulations (LH, RCP85 and PI_{GH}) with the PI control, with respect to temperature (Fig. 2). Although there are slightly different orbit configurations between the PI, LH, and RCP85, it is useful to compare these three simulations with the PI_{GH} simulation, as one would expect the temperature changes to fall in a linear series to account for the logarithmic response of greenhouse gases. However, the spatial pattern of temperature changes is not linear. The LH simulation has warm spots over Hudson Bay, the southern coast of Greenland, and areas in the Arctic, but is cooler at lower latitudes (Fig. 2a). The RCP85 simulation has a large hotspot over the Arctic Ocean, and general global warming amplified over land (Fig. 2b). However, when greenhouse gases are lowered in the PI_{GH}, the cold spots do not always correspond to the warm spots in the RCP85 simulation, as in the PI_{GH} there is a cold spot in the Pacific Northwest and in the Arctic Ocean north of Scandinavia ($>16°C$, Fig. 2c). These cold spots are expected as they correspond to the sea ice edges where polar amplification is the main driver.

Already we see that the climate system is complex and not responding in a linear, predictable fashion. Further complicating the non-linear responses is a series of sensitivities teasing apart the impacts of orbit, Greenland ice sheet height, and greenhouse gases. When the orbit is substantially changed to the LGM configuration (Table 1; PI_{ORB}), we see warming over the North American continent and strong cooling over the Bering Strait and between Greenland and North America (Fig. 2d; PI_{ORB}). When raising the Greenland ice sheet to 125% height (Fig. 1; PI_{GL}), there is the expected adiabatic cooling over Greenland, but a warming in North America and a cooling over the Bering Strait (Fig. 2e). When combining the orbit change with the Greenland ice sheet increase ($PI_{ORB,GL}$), we see the expected adiabatic cooling in Greenland. Additionally, North America warms whereas there is a cooling in the Bering Strait and Arctic Ocean (Fig. 2f). Combining the orbit, greenhouse gases, and ice sheet height ($PI_{ORB,GL,GH}$), we see overall global cooling (dominated by the greenhouse cases), with the largest cooling in the Arctic Ocean north of Scandinavia and the Pacific Northwest (Fig. 2g). Finally, we show the relative impact from the simulations with single boundary condition changes, either orbit or ice sheet, and adding them together while comparing them to the simulations that combine orbit and ice sheet boundary condition changes ($PI_{ORB} + PI_{GL} - PI_{ORB,GL}$). If the climate system responded linearly, these effects would cancel each other out. However, we see an enhanced warming over the North American continent and in the ocean east of Greenland, while there is enhanced cooling in the Bering Strait (Fig. 2h). Adding an additional layer of complexity ($PI_{ORB} + PI_{GL} + PI_{GH} - PI_{ORB,GL,GH}$), we see warming on the North American continent ($\sim 3°C$). The coast of Newfoundland cools by $>16°C$, to the east of Greenland there is $>4°C$ of warming, and the Bering strait cools by $8°C$ (Fig. 2i). We show evidence that the combined changes of orbit, ice sheet height, and greenhouse gases for glacial climates will return non-linear effects that are not explained by the individual changes alone.

https://doi.org/10.5194/egusphere-2023-324
Preprint. Discussion started: 6 March 2023

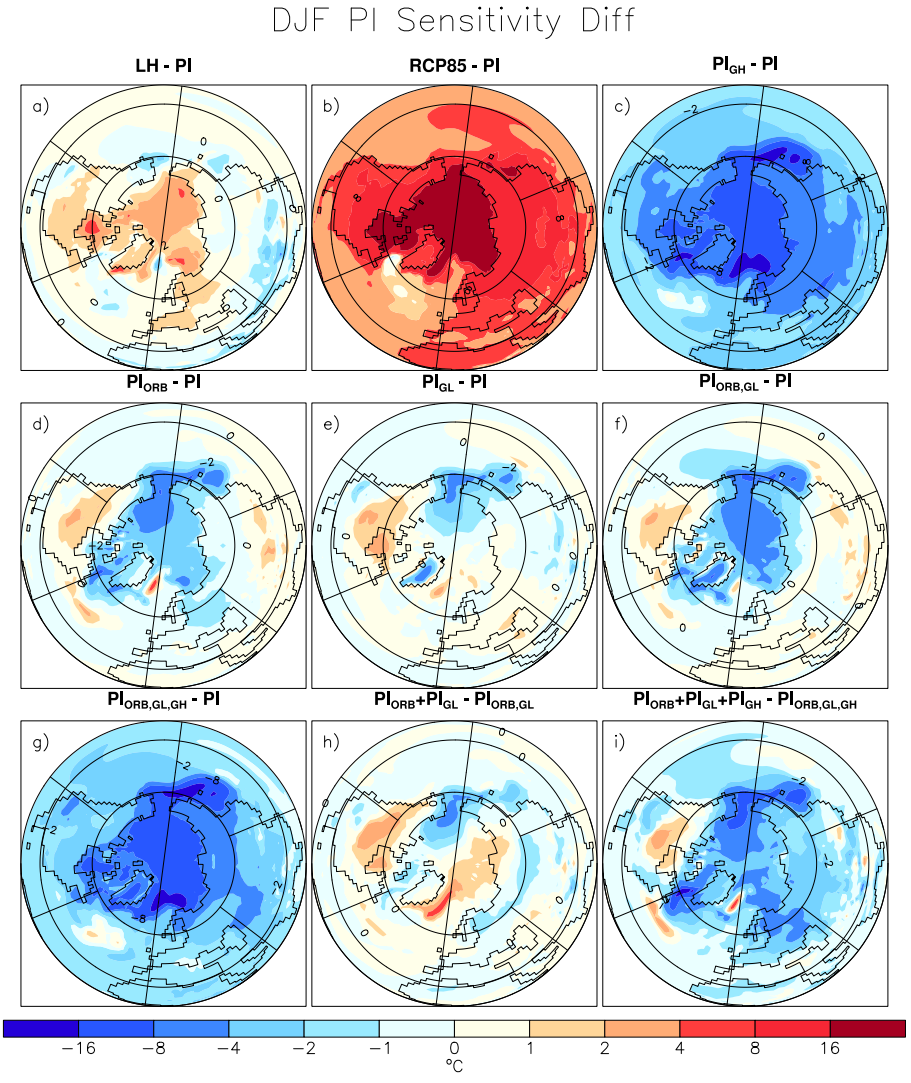

Figure 2. Northern Hemisphere surface temperature response for 7 different boundary changes with respect to the preindustrial (PI) control. Shown is the difference between (a) Late Holocene and PI, (b) last 20 years of the 21st century (RCP85) and PI, (c) LGM greenhouse gas (PI_{GH}) concentration and PI, (d) LGM orbital configuration (PI_{ORB}) and PI, (e) Greenland height (PI_{GL}) increase to 125% and PI, (f) LGM orbital configuration combined with Greenland height increase to 125% ($PI_{ORB,GL}$) and PI, (g) combination LGM orbit, Greenland icesheet, and greenhouse gases ($PI_{ORB,GL,GH}$ and PI. In panel (h), we show the difference between (d) plus (e) and (f) and in panel (i) the difference between (c) plus (d) plus (e), and (g) is shown to illustrate the nonlinearity of the combined responses.

Likewise, precipitation is a critical companion to temperature changes in paleoclimate simulations (Fig. 3); therefore, evaluating precipitation changes in this Preindustrial sensitivity suite is just as crucial. Except for an increase by coastal Western Europe and the Iberian Peninsula, the Northern Hemisphere precipitation from the LH shows enhanced precipitation (Fig.

https://doi.org/10.5194/egusphere-2023-324
Preprint. Discussion started: 6 March 2023

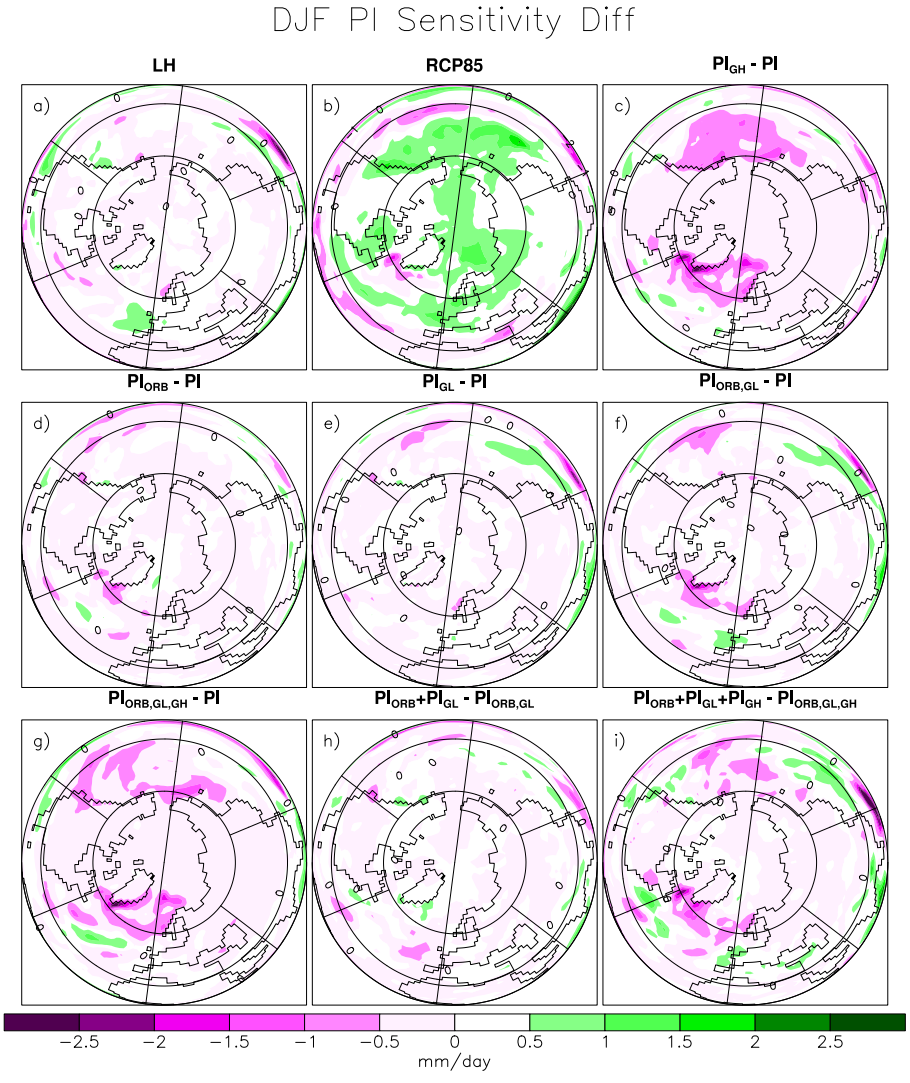

Figure 3. As Fig.2, but for precipitation.

3a). Otherwise, Northern Hemisphere precipitation in winter changes very little, and the rate of precipitation globally decreases slightly. Greenhouse gases, however, have a strong precipitation response. Because of the warming atmosphere and the Clausius-Clapeyron temperature-moisture relationship (Agard and Emanuel, 2017), the RCP85 simulation (Fig. 3b) shows precipitation increasing most broadly over the Northern Pacific and Arctic Oceans, a precipitation decrease to the south of
225 Greenland, and a strong belt of increased precipitation in the Northern Atlantic that continues to Europe and Northern Asia. However, although lowering greenhouse gases (PI_{GH}) does produce a drop in precipitation, the spacial pattern of that change is not a one-to-one relationship with the RCP85 (Fig. 3c). In both cases, greenhouse gases are well mixed, and a unique pattern represents a non-linear change in precipitation behavior.

https://doi.org/10.5194/egusphere-2023-324
Preprint. Discussion started: 6 March 2023

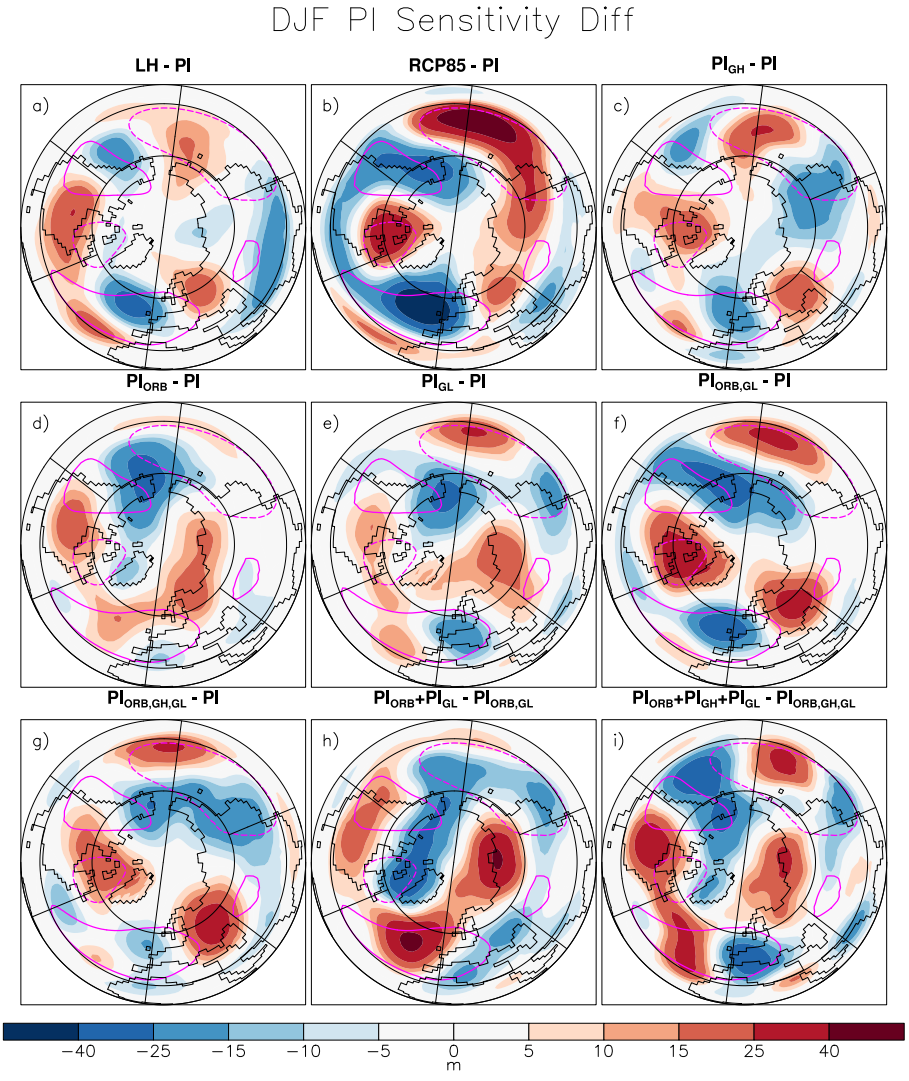

Figure 4. As Fig.2, but for geopotential height at 500 hPa with the zonal mean removed (shading). The contours show the mean geopotential height at 500 hPa with the zonal mean removed of the PI Control (sold contour represents the positive 80 gpm geopotential height and dashed is the negative -80 gpm geopotential height).

Combining orbit and ice sheet changes further demonstrates the non-linear nature of atmospheric responses and their locations. Changing the PI orbit induces a small reduction in precipitation globally, but there are still regional responses as well. For example, there is a 1-2 mm/day reduction in rainfall south of Greenland (Fig. 3d). Raising the ice sheet height (PI_{GL}), the larger amplitude changes occur in the North Pacific, with +0.5 mm/day in the west and -0.5 mm/day is the east (Fig. 3e). Combining orbit change and ice sheet (as seen in $PI_{ORB,GL}$) amplifies the effect more than the individual components (Fig. 3f). Although the decrease in precipitation to the south of Greenland has a small response in the PI_{GL}, the combined orbit and ice

https://doi.org/10.5194/egusphere-2023-324
Preprint. Discussion started: 6 March 2023

sheet experiment results in a greater loss than the two simulations that change ice and orbit alone. Combining the LGM orbit with Greenland icesheet and greenhouse gasses ($PI_{ORB,GL,GH}$), there are regional decreases in precipitation in the North Atlantic and North and Eastern Pacific (Fig. 3g). If these changes were linear, the addition of each simulation with individual changes would be equal to the simulation that incorporated each boundary condition together. However, the sum of the simulations with single changes does not equal the simulation with all of the changes (Fig. 3h). When comparing the individual orbit and Greenland ice sheet simulations to the combined simulation, the North Pacific has an amplified loss of precipitation (>2.5 mm/day), as does Eurasia, whereas the Arctic Ocean sees a strong increase in precipitation response. Further complicating the picture is that instead of two changes, three changes are made to a single simulation (orbit, ice, and greenhouse gasses) versus the simulations with individual components (Fig. 3i). Losses in precipitation are amplified over most of the Northern Hemisphere except for northern North America and the Northwest Atlantic.

Finally, we assess the changes in atmospheric circulation between each sensitivity simulation and the PI (Fig. 4). We use the 500 hPa geopotential height field, removing its zonal means, to extract the behavior of stationary waves. The LH period shows the orbit's influence on the high-low pressure zones, dampening stationary waves over the Northern Pacific, creating an extended high-pressure zone over North America, a high-pressure north-south intensification in the North Atlantic, and expanding high pressure further east over Northern Europe (Fig. 4a). Increasing greenhouse gases in the RCP85 simulation, we see a hemispheric wide dampening of atmospheric pressure anomalies (Fig. 4b); curiously, the decrease in greenhouse gasses (PI_{GH}) has a similar overall hemispheric dampening of the stationary waves as in RCP85, except for an intensification over North Eastern Asia (Fig. 4c).

Each of the individual sensitivities (PI_{GH}, PI_{ORB}, PI_{GL}, Fig. 4c-e, respectively) shows unique spatial changes. The PI_{ORB} has an expansion and intensification of the pressures anomalies (Fig. 4d), but the PI_{GL} ice sheet increases cause a north-south dampening of stationary waves in the Pacific while creating enhanced stationary waves in the North Atlantic, as well as a northerly expansion of pressures anomalies over North Central Asia (Fig. 4e). The combination of ice sheet and orbit changes ($PI_{ORB,GL}$) cause a strong dampening of the stationary waves where the low-pressure zones (dashed lines) have positive pressure anomalies, and the high-pressure zones (solid lines) have negative pressure anomalies (Fig. 4f). Adding in the greenhouse gasses ($PI_{ORB,GL,GH}$), there is an eastward shift of the low-pressure zone in the North Pacific and the high-pressure zone over Europe expands westward (Fig. 4g). In terms of non-linear changes, similar to the impacts on temperature and precipitation, the stationary anomalies do not reflect the sum of the individual parts (Fig. 4h and i). Comparing the combined effects ($PI_{ORB,GL}$), strengthens the atmospheric structures as compared to the individual components (Fig. 4h). When adding in the greenhouse gases ($PI_{ORB,GL,GH}$), there is an enhanced dampening from the Northern Pacific to North America, an intensification and tightening of the North Atlantic structure, and a northward expansion of the Northern Asia high zone (Fig. 4i).

3.2 Evaluation of the simulated LGM climate state

After contextualizing the behavior of the Preindustrial climate, we move to paleoclimate periods (the LGM), and, as in the previous section, we generate a framework for comparing each paleoclimate simulation. To that end, we evaluate the LGM to the PI by comparing the recent reanalysis reconstruction and our simulations. To remove systematic deficiencies, a common

https://doi.org/10.5194/egusphere-2023-324
Preprint. Discussion started: 6 March 2023

approach for evaluating different climate states is assessing the simulated response behavior rather than evaluating the absolute values (Stocker et al., 2013). Here, we follow this approach and compare anomalies between the LGM and the PI generated by the CESM simulations that we executed, with the anomaly generated between the LGM and the PI based on proxy data and observation reanalysis products. For proxy data, we rely on several major sources. Pollen-based proxies provide estimates of precipitation and temperature at sites on the continents (Bartlein et al., 2011). Similarly, ice core data provides temperature information on ice sheets; particularly relevant are the Greenland ice cores due to their proximity to Europe. And proxies from sediment cores provide information of sea surface temperatures (Waelbroeck et al., 2009; Tierney et al., 2020b).

A first overview uses the global mean estimates of the temperature amplitude between the LGM and the PI provided by the Paleoclimate Modeling Intercomparison Project, PMIP (Annan and Hargreaves, 2013; Holden et al., 2009; Schneider von Deimling et al., 2006; Tierney et al., 2020b). CESM falls within the range of several proxy reconstructions that are used by PMIP (Schneider von Deimling et al., 2006; Holden et al., 2009). The simulated global mean temperature difference is -6.3°C. While the temperature difference is larger than the range of -4.8°C to -3.2°C from the most recent reconstruction (Annan et al., 2022), our results are within a recent proxy reconstruction estimate, ranging from -6.5°C to -5.7°C (Tierney et al., 2020b).

Another comparison to proxy data is presented in Fig. 5. Here, we focus on two sea surface temperature (SST) reconstructions (Rayner et al., 2003; de Vernal et al., 2006). The reconstructions and the simulation show the expected cooling response when comparing the PI and the LGM conditions. The SST from our CESM LGM simulations is slightly colder in the tropics than the MARGO reconstruction (Waelbroeck et al., 2009). In the North Atlantic region there is a warm bias, but given the range of uncertainty with MARGO's data (not shown), which has values of up to +/- 4°C, the CESM simulation is still within this range. The comparison to the Tierney reconstruction confirms this finding (Fig. 5), so that a slight warm bias in the North Atlantic from the CESM simulation might be possible. Overall, our CESM LGM realistically simulates the amplitudes between the PI and the LGM from reconstructed SSTs. Even given recent reconstructions' uncertain ranges, the SST patterns during the LGM agree with the reconstructions in general, as the model simulates glacial climate states, and in particular, the large scale features.

3.3 Quaternary sensitivity to orbital forcing

Here we shift from demonstrating non-linear changes to the PI environment to evaluating the LGM's sensitivity with respect to orbit changes. We specifically focus on recent periods of glacial maxima, known as the evenly numbered Marine Isotopic Stages (MIS). Like the analysis of the PI sensitivity simulations, we concentrate on temperature (Fig. 6), precipitation (Fig. 7), and 500 hPa geopotential height anomalies (Fig. 8). The control orbit condition is the LGM, while the orbit of each Marine Isotopic Stage are the sensitivity simulations. The ice sheet heights are isolated from this analysis by using the LGM orbit simulation with the same ice sheet height as the MIS sensitivity simulation. If the impacts of the ice sheet were linear with orbit changes, we expect that each variables' anomalies would be the same, regardless of ice sheet heights. However, our results disprove this hypothesis. We repeat this analysis with fixed ice sheet changes within one specific orbit (Fig. 9-11). Like the sensitivity simulations for the PI, the climate system under paleo conditions is state dependent.

https://doi.org/10.5194/egusphere-2023-324
Preprint. Discussion started: 6 March 2023

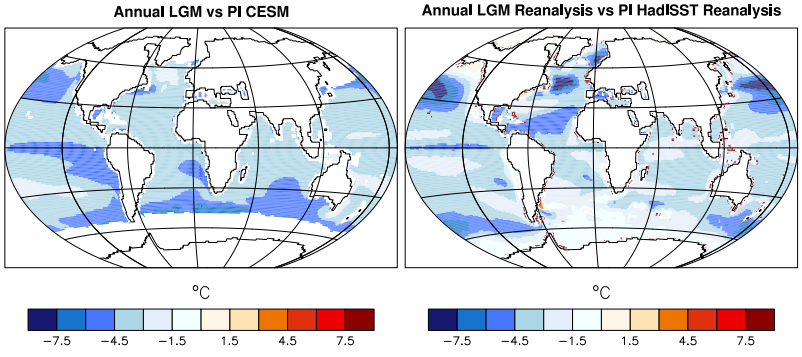

Figure 5. Comparison of the sea surface temperature response between LGM and PI using (a) the CESM and (b) reanalyses products. For the LGM reanalysis we use Tierney et al. (2020b) and for the PI reanalysis Rayner et al. (2003).

Temperature changes between orbits can cool or warm icehouse conditions. MIS4 shows a strong land cooling in the Northern Hemisphere (Fig. 6a-d), whereas MIS6 shows high latitude warming (Figs. 6e-h). Meanwhile, MIS8 has a combination of high latitude warming and lower latitude cooling (Figs. 6i-l). This is a general outlook of the temperature changes; however, there are feedbacks with ice sheet heights. Arctic temperatures reverse sign between I125 (Fig. 6a) and the other three ice sheet heights in MIS4 (Figs. 6b-d). But at lower ice heights (I067 and I033), temperatures warm in the Northern Pacific by 1°C to

https://doi.org/10.5194/egusphere-2023-324
Preprint. Discussion started: 6 March 2023

4°C (Figs. 6c-d) as compared to the higher ice sheets (I100 and I125; Figs. 6a-b). In MIS6, the ice height secondary effects are dampened by the orbital signal, as only the I100 case (Fig. 6f) shows hemispheric cooling (excluding North America), and for all other ice sheets there is substantial warming (Figs. 6e, g, and h). Like MIS4, the MIS8 conditions show cooling (Figs. 6I and j), but at the lower ice sheet heights (I067 and I033; Figs. 6k and l) the Northern Pacific, parts of the Arctic, and Europe become warmer.

The orbit influences precipitation changes in select regions of the Northern Hemisphere. What is unique about the LGM configuration is that there is a consistent Northern Hemispheric drying. There is a strong decrease in rainfall between MIS4 and LGM off the eastern coast of North America by 1 mm/day (Figs. 7a-d). For MIS6, rainfall in the Northeastern Pacific consistently intensifies (Figs. 7e-h). Finally, MIS8 shows drying off the Northeastern coast of North America (Figs. 7i-l). However, as with temperature, there are specific changes that ice sheet height dependency imposes on these rainfall patterns. In the Northeastern Pacific, drying only intensifies at low (I033) and moderate (I100) ice sheet heights (Figs. 7b and d). For MIS6, there is a strong east-west dry-to-wet pattern off the coast of Europe that only shows up in I100 (Fig. 7f). As the ice sheet shrinks, the Western Pacific becomes drier by 1 to 1.5 mm/day (Figs. 7g and h). A high ice sheet (I125 and I100) has a wet effect on the Eastern Atlantic for MIS8 (Figs. 7i and j) and there is a consistent wet zone of 0.5 to 1 mm/day in the East Pacific for high (I125) and low (I067) ice sheets (Figs. 7i and k).

The stationary wave patterns, illustrated by the 500 hPa geopotential height anomalies and with its zonal mean removed, also reveal orbit influences during glacial maxima (Fig. 8). Using the I100 experiments, we find a strong dampening of the stationary wave in the North Pacific for MIS4 and a weakening of the wave train over North America (Fig. 8b). Over the North Atlantic, the negative anomalies of stationary wave pattern are displaced southward and the positive anomaly over Europe is enhanced. MIS6 shows a reverse behavior over the North Pacific compared to MIS4, enhancing the negative anomaly, while the eastern wave train across North America becomes weaker (Fig. 8f). Over Europe the stationary waves are mainly enhanced. MIS8 agrees with MIS4 in the North Pacific, showing a dampening of the negative anomaly, but the wave train over North America is displaced westwards (Fig. 8j). The North Atlantic and Europe share a similar structure as MIS6. The stationary waves dependency on orbit responses to different ice sheet heights is evident when comparing the I100 patterns to I125, I067, and I033. The North Pacific shares similar patterns for MIS4, MIS6, and MIS8 for I100, I067, and I033, but no clear sign reversal for I125, as east-west dipole anomalies are found instead. Over the North Atlantic and Europe there is no common behavior, highlighting the non-linearity of the circulation response to orbital forcing with respect to ice sheet heights in this region. For example, in some cases the ice sheet dampens the Northeastern America low pressure zone (Figs. 8e and f) or causes no changes (Figs. 8g and h). Thus, depending on the ice sheet height, continent spanning high-pressure zones can be dampened or intensified, a non-linear change linked to ice sheet heights.

3.4 Quaternary sensitivity to Northern Hemisphere ice sheet height

Shifting towards the sensitivities to ice sheet changes with a fixed orbit, we continue to see the interplay between ice sheets and orbital changes, where the structural influence of the ice sheet dominates the orbital changes. Our analysis keeps the orbit fixed between simulations but always subtracts the default I100 ice sheet.

https://doi.org/10.5194/egusphere-2023-324
Preprint. Discussion started: 6 March 2023

Temperature changes are the easiest to analyze in terms of ice sheet heights (Fig. 9). Starting with the high ice sheet (I125), cooling occurs over the Laurentide Ice Sheet and Fennoscandiavian sheet (Figs. 9a-d), which is expected due to adiabatic lifting from the ice sheet's increased height. All the simulations demonstrate regional strong warming over the Northern Pacific, warming on the Eastern Peninsula of North America, and cooling over Eastern Europe. However, although the orbital conditions are fixed, there are differences that appear between the simulations. The LGM and MIS4 orbits show cooling over Western Europe (Figs. 9a and b), whereas MIS6 and MIS8 show Western Europe becoming wamer (Figs. 9c and d). The LGM has almost no warming in southwestern North America (Fig. 9a), whereas MIS4, MIS6, and MIS8 clearly reveal a warmer southwest (Figs. 9b, c,and d). Finally, both MIS6 and MIS8 show warming in Central Asia (Figs. 9c and d).

Lowering the ice sheet leads to adiabatic compression and local warming over the ice sheets. Though counter intuitive, lowering the ice sheet (I067) cools the climate's global mean temperature regardless of orbit (Figs. 9e-h). For example, the Northern Pacific becomes cooler, as does the Northeastern North American Peninsula. However, there are non-linear changes due to orbit that come through. In Europe, within the LGM, there is almost no change in temperature (Fig. 9e), whereas MIS4, MIS6, and MIS8 show warming (Figs. 9f, g, and h). But, as the ice sheet is lowered further (I033), the warming over Europe is consistent between all simulations (Figs. 9i-l). The largest differences between the orbits is seen in the North Atlantic, which has a warm spot off Newfoundland for the LGM, MIS4, and MIS8 but no change in MIS6 (Figs. 9i, j, and l).

The impacts of ice sheet heights on precipitation are shown in Fig. 10. The high ice sheet (I125) increases precipitation relative to I100 in the Eastern Pacific (Figs. 10a-d) and in the Northern Pacific, while precipitation decreases in the Northeast Pacific along the northern coast of North America. Europe's West Coast has positive and negative precipitation rates between different orbits relative to the high ice sheet. In particular, the LGM and MIS4 show coastal drying of 0.5 to 1 mm/day (Figs. 10a and b), and coastal precipitation increases of 0.5 to 1 mm/day in MIS6 and MIS8 (Figs. 10c and d). But these orbits are not consistent everywhere; the LGM and MIS6 have increased precipitation in the Southeastern North America (Figs. 10a and c) that is not reflected in MIS4 and MIS8 (Figs. 10b and d).

Like with temperature, as the ice sheet lowers, ice sheet driven precipitation changes regardless of orbit. The wet Eastern Pacific becomes dryer (Figs. 10e-h), and dry coastal Northwest America receives more precipitation. A drying effect occurs just off the coast of the Northeast America, while the Western Pacific has a consistent precipitation increase. Europe, however, like with temperature, changes inconsistently. There is drying off the Iberian Peninsula, but the North Atlantic shows increased precipitation for the LGM, MIS6, and MIS8 (Figs. 10e, g, and h) but not MIS4 (Fig. 10f). As the ice sheet is lowered further (I033), the Eastern Pacific becomes even drier while in the Western Pacific precipitation increases (Figs. 10i-l). The orbital influences described for I067 apply to I033, with the North Atlantic showing increased precipitation for the LGM, MIS6, and MIS8 (Figs. 10i, k, and l) but not MIS4 (Fig. 10j). Thus, precipitation has strong structural features that are consistent between different fixed orbits, demonstrating the dominance of the ice sheet height sensitivity on precipitation.

The response of atmospheric circulation to ice sheet height changes is again assessed using the 500 hPa geopotential height anomaly removing its zonal mean (Fig. 11). Increasing the height of the ice sheets shows that the baseline structure for the four different orbits are similar (pink lines), with a low pressure zone over Northeastern North America, Northern Asia, and the Northwestern Pacific. The high-pressure structure is found in Northwestern North America, stretching from the East Coast

https://doi.org/10.5194/egusphere-2023-324
Preprint. Discussion started: 6 March 2023

of North America through Europe and into Central Asia. The low pressure over Northeastern North America is weakened in all orbits, while high pressure strengthens over the west coast of Europe in the LGM, though in MIS6 this increase weakens (Figs. 11a and c). Still, the orbital influences are rather strong. The LGM, MIS4, and MIS8 states shows the stationary waves dampening over Eastern Europe, and Northern Asia's low intensifying (Figs. 11a, b, and d). In the LGM, the Eastern Pacific low pressure becomes broader and becomes weaker over the Northwestern North America (Fig. 11a).

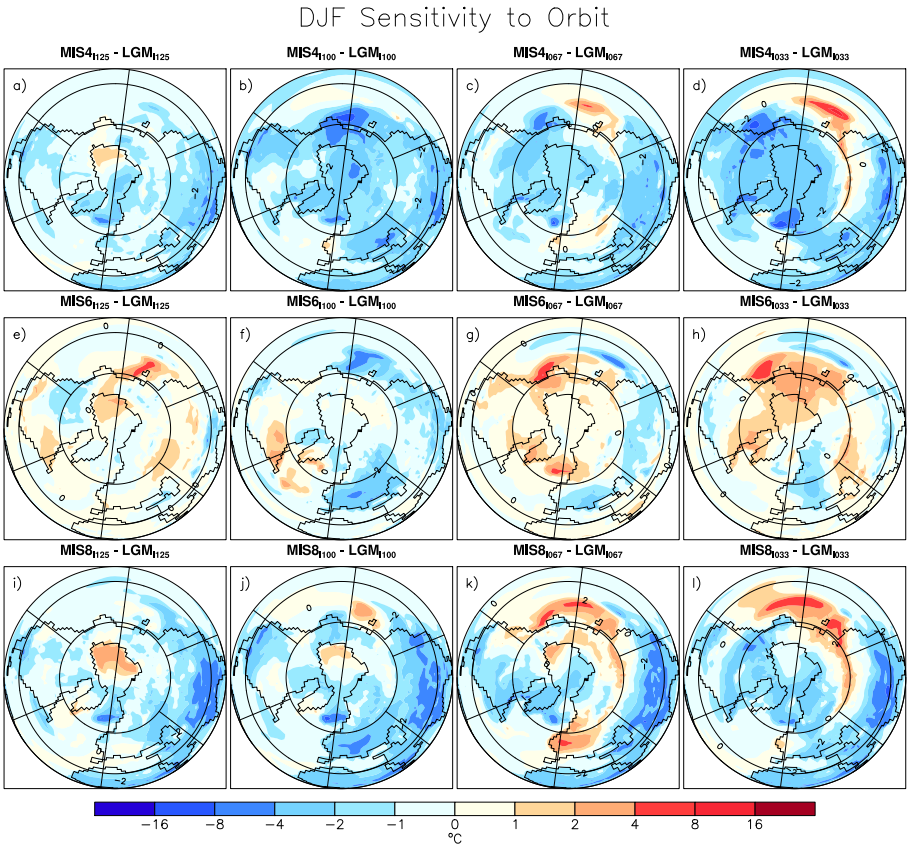

Figure 6. Northern Hemisphere surface temperature response to different orbital configurations. Differences are calculated between the MIS and the corresponding LGM simulation: (a-d) MIS4, (e-h) MIS6, and (i-l) MIS8. Columns are for different Northern Hemisphere ice sheet heights: 125%, 100%, 67% and 33% (left to right).

However, regardless of orbit, when the ice sheet is lowered (I067) the structures become fixed. The high pressure over the Atlantic is strengthened, specifically in the LGM, MIS6, and MIS8 (Figs. 11e, g, and h), and in contrast to MIS4, the high pressure over the Atlantic expands northward (Fig. 11f). Additionally, the high pressure over Europe intensifies in MIS4, MIS6, and MIS8 (Figs. 11f, g, and h). Otherwise, the rest of the globe shows a dampening of the stationary waves, regardless of whether the location is a high- or low-pressure zone. For example, the Northern Pacific shows an increase in pressure, dampening the low-pressure zone (Figs. 11e-h), at the same time the high pressure over Northwestern North America is

https://doi.org/10.5194/egusphere-2023-324
Preprint. Discussion started: 6 March 2023

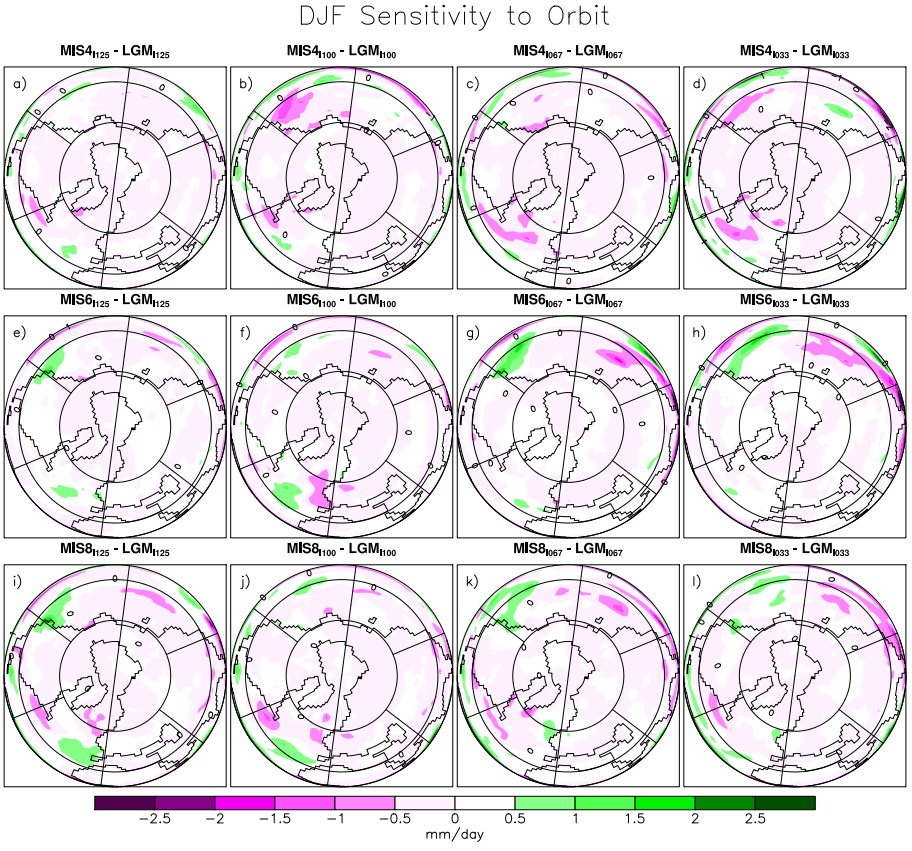

Figure 7. As Fig. 6, but for precipitation difference.

reduced. There is a weakening of the high pressure off the East Coast of North America (Figs. 11e-h). Shifting to Asia, the northern low is dampened by an increase in pressure (Figs. 11e-h). If the ice sheet is lowered further, all of these structures previously described in I067 are further enhanced except for the high pressure weakening over the eastern coast of North America in MIS6 rather than over the whole Atlantic region as in LGM, MIS4, and MIS8.

4 Discussion

Paleoclimate modelers use sensitivity studies to identify and understand the underlying processes of climate system (Merz et al., 2014a; Acosta et al., 2022). However, to reduce computational expense, Earth system modelers tend to only evaluate changes between one climatic time period and the Preindustrial (Zhu et al., 2017). Our baseline simulations (PI and LGM_{I100}) were already evaluated for scientific quality and we do not discuss them further (Zhu et al., 2017; Tierney et al., 2020b). Instead, we demonstrate the added value of using fully coupled sensitivity simulations to evaluate the Preindustrial and Quaternary climate states.

https://doi.org/10.5194/egusphere-2023-324
Preprint. Discussion started: 6 March 2023

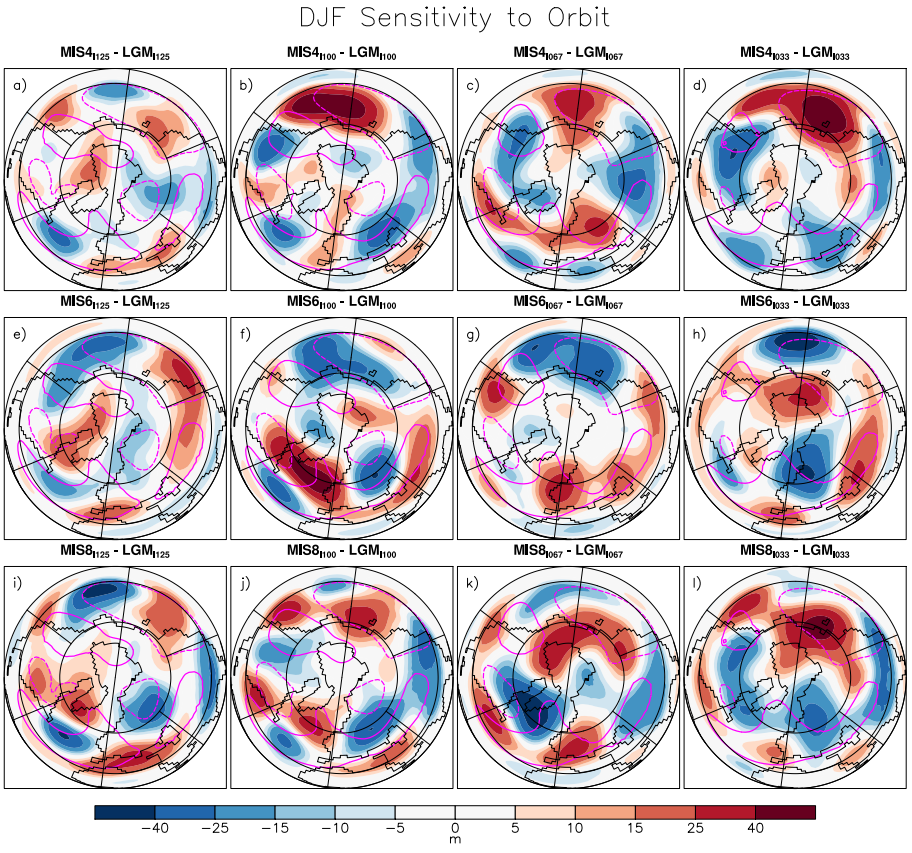

Figure 8. As Fig. 6, but for geopotential height at 500 hPa with the zonal mean removed. The contours show the mean geopotential height at 500 hPa with the zonal mean removed of the PI Control (positive is solid and negative is dashed).

4.1 Preindustrial sensitivity analysis

Making sensitivity changes to Preindustrial climate conditions is not new. Recent work uses CAM4 driven by SSTs from CCSM3 to modify the PI climate system with LGM ice sheets (Merz et al., 2015) and evaluate the Eemian warm state using PI Greenland ice sheets (Merz et al., 2014a, b). Our PI sensitivity experiments show that Greenland ice sheet modifications and greenhouse gas modifications resolve in non-linear changes of surface temperature (Fig. 2). Likewise, modifying the ice sheet in the PI and the Eemian experiments also demonstrates non-linear lapse rate changes inconsistent with direct altitude changes (Merz et al., 2014b). This is also consistent with our PI sensitivities, showing that combinations of orbit, greenhouse gases, and Greenland ice sheet changes do not linearly combine (Fig. 2). Unfortunately, these previous sensitivity studies (Merz et al., 2014a, b) do not include precipitation changes for a comparison with ours, but we suspect that given the non-linear changes in temperature there would be non-linear changes in precipitation as compared to our sensitivities as well (Fig. 3). Imposing the LGM icesheets on the PI boundary conditions strongly changes the stationary wave patterns in the atmosphere, confirmed in the MIS4 orbital conditions (Merz et al., 2015). Our simulations, which include the reactions from a

https://doi.org/10.5194/egusphere-2023-324
Preprint. Discussion started: 6 March 2023

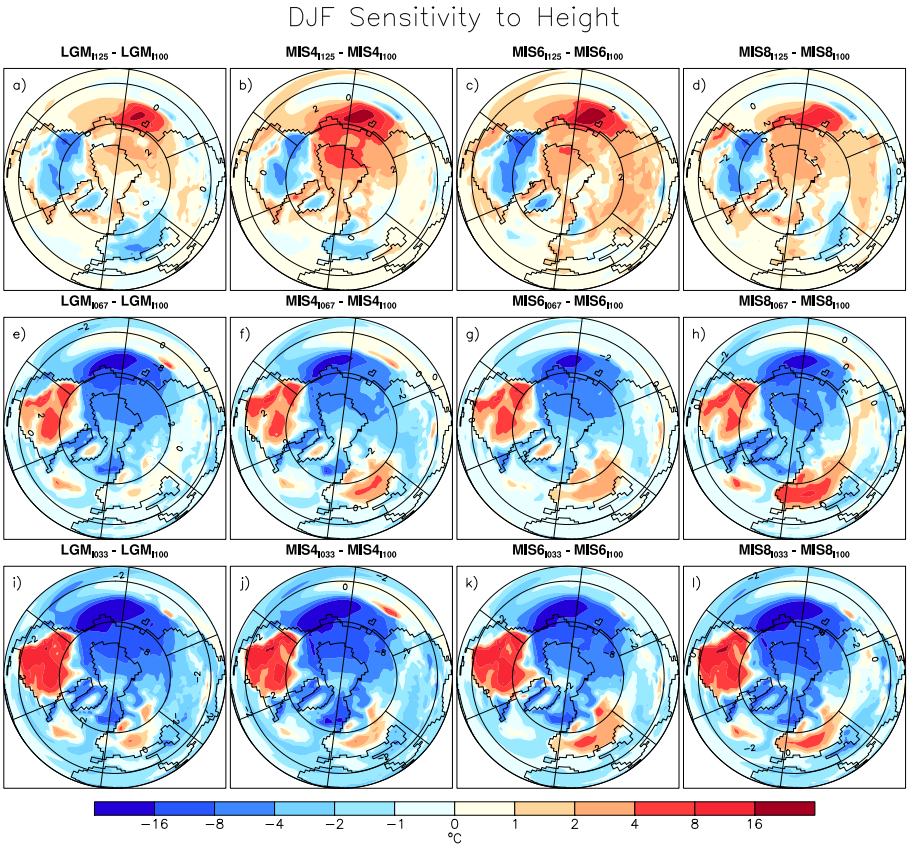

Figure 9. Northern Hemisphere surface temperature response to different Northern Hemisphere ice sheet heights. Differences are calculated between the different heights and the configuration with 100% ice sheet height within one glacial state: (a-d) 125%, (e-h) 67% and (i-l) 33%. Columns are for different orbital configuration: LGM, MIS4, MIS6, and MIS8 (left to right).

fully coupled ocean, demonstrate that the stationary patterns in geopotential height are enhanced when comparing ice sheet and orbit changes individually versus our simulation that includes both (Fig. 4). These sensitivity simulations, utilizing imposed SSTs, demonstrate that there are non-linear structural changes to the atmosphere, but that their magnitudes may be incorrect as they are not coupled to the ocean.

4.2 Quaternary sensitivity analysis

To date, our experimental framework is the most extensive use of fully coupled sensitivity simulations for CESM in the Quaternary climate period. The 16 simulations represent networks of orbit and ice sheet configurations at a level of detail and complexity unparalleled in previous uses of CESM. As such, we can make few direct comparisons between our work and previous studies results, since previous CESM studies evaluated only the LGM and MIS4 icehouse states. However, we

https://doi.org/10.5194/egusphere-2023-324
Preprint. Discussion started: 6 March 2023

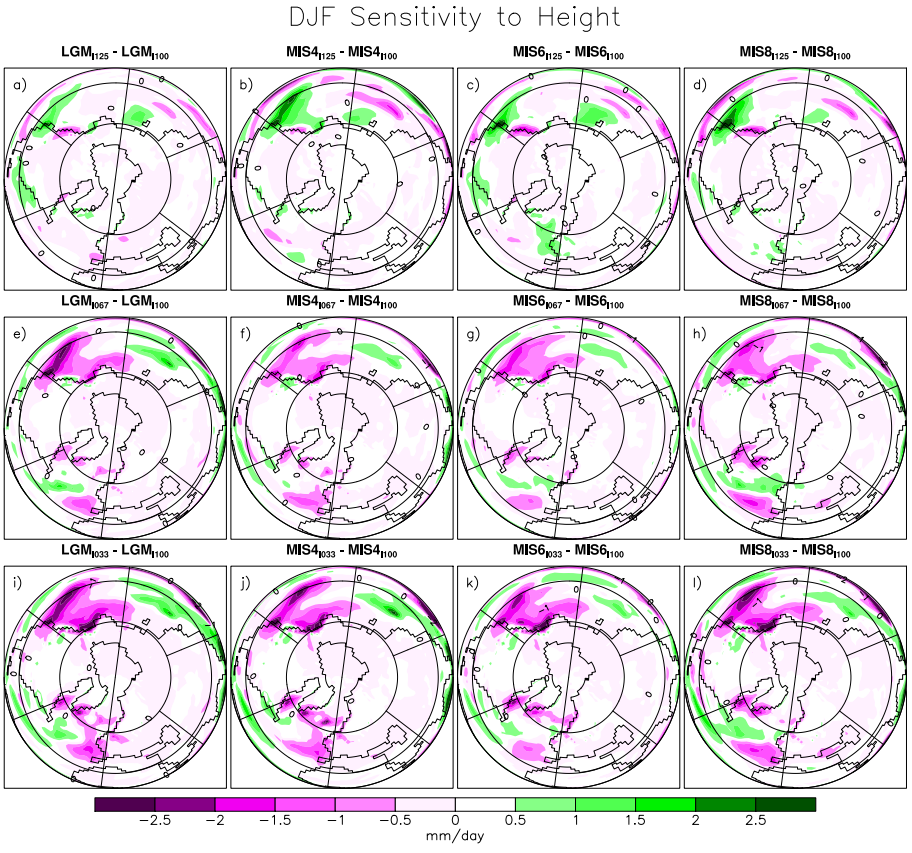

Figure 10. As Fig. 9, but for precipitation.

can compare these two sets of experiments that offer the closest comparison to our experimental framework using slab ocean (ocean heat flux) or fixed SST simulations. Below, we compare those simulations with our results.

The first set of studies was conducted using CAM3 in a slab ocean configuration (Löfverström et al., 2016; Liakka and Löfverström, 2018), with scale factors of 0.5 to 1.5 (Löfverström et al., 2016). This is like our experiments, where we use 0.33, 0.67, 1., and 1.25, where 1 is the same as I100 LGM ice sheet (Peltier et al., 2015), although the use of a slab ocean model can have a strong impacts on the atmospheric circulation (Raible and Blender, 2004). However, increasing the ice sheet height leads to 300 hPa zonal winds becoming stronger (Löfverström et al., 2016; Liakka and Löfverström, 2018), as well as increasing areas of stationary wave structures. Analogously, we look at geopotential height changes with the zonal anomaly removed, which is a measure for stationary waves (Fig. 11). At higher ice sheet heights, our structure becomes broader (Fig. 11a), and as the ice sheet is lowered, the geopotential height structure becomes weaker (Figs. 11e and i). We show that although the spatial patterns are different between orbits, the intensification of geopotential height zones is a robust feature across ice sheet height increases (Fig. 11). In the second study, the Laurentide Ice Sheet is scaled by a factor of 0 (Preindustrial) to 1.25 (which is approximate to Peltier et al. (2015) LGM ice sheet) in 0.25 increments. This study focuses on temperature changes

https://doi.org/10.5194/egusphere-2023-324
Preprint. Discussion started: 6 March 2023

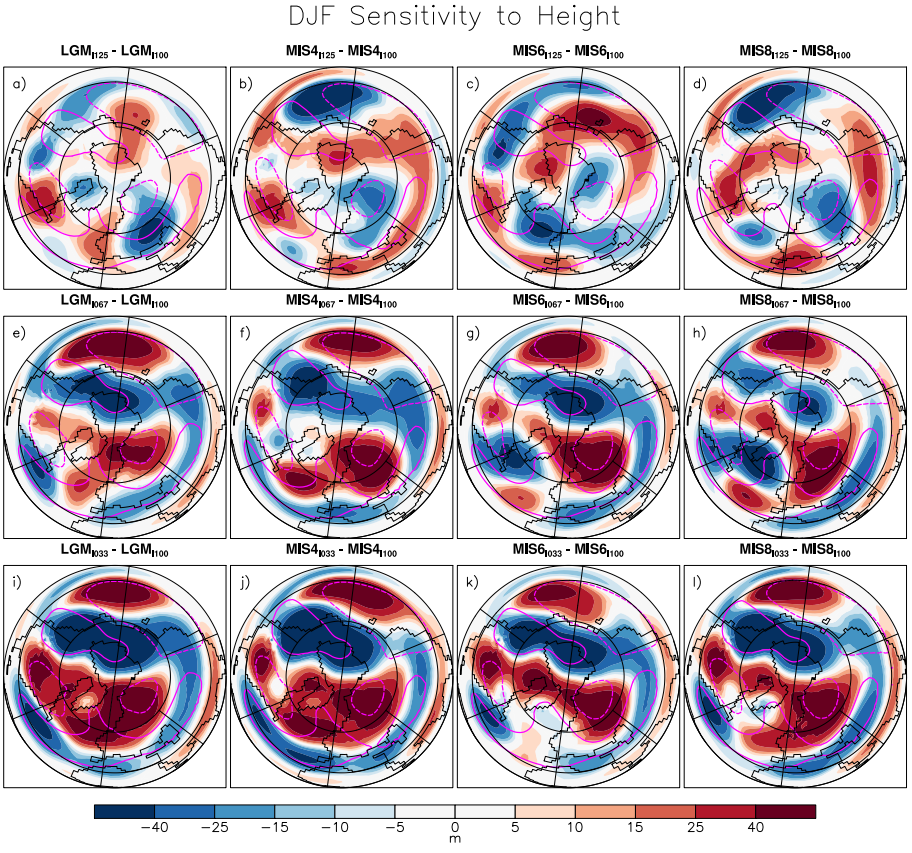

Figure 11. As Fig. 9, but for geopotential height at 500 hPa with the zonal mean removed. The contours show the mean geopotential height at 500 hPa with the zonal mean removed of the subtracted field (positive is solid and negative is dashed).

in the Artic related to topographical changes. Here, the authors showed that as ice sheet height increases, the temperature in the Arctic increases as well. Likewise, in our fully coupled simulations, we show a similar pattern of the Arctic's temperature increasing with increases in ice sheet height (Figs. 9a, e, and i). Furthermore, this temperature pattern is consistent across orbital configurations (Fig. 9). These results imply a strong climate negative feedback as ice sheet height increases that is further confirmed by our global mean surface temperatures, which are impacted by ice sheet height. For example, the LGM_{I033} and LGM_{I067} are -1.85°C and -1.31°C colder, respectively, than the LGM_{I100}, and the LGM_{I125}, which is 0.16°C warmer.

Comparing our MIS4 orbital simulations, previous studies utilized CAM4 driven by SSTs from the CCSM3 fully coupled simulation (Hofer et al., 2012b, a; Merz et al., 2015). In their simulations, the ice sheet was set to an earlier version of the LGM ice sheet reconstruction (Peltier, 2004), and the Laurentide Ice Sheet was scaled by a factor of 0.46, 0.67, 1., and 1.25. An additional experiment scaled the Fennoscandinavian Ice Sheet by 0.33 (0.76 for the Laurentide). Similar to the LGM simulations with ice sheet height changes, the low level zonal winds in the MIS4 simulations increase in intensity as the ice sheet height increases (Merz et al., 2015). Additionally, the 300 hPa zonal winds become more intense with ice sheet increases,

https://doi.org/10.5194/egusphere-2023-324
Preprint. Discussion started: 6 March 2023

regardless of the orbit conditions (Merz et al., 2015) or the version of CAM (Löfverström et al., 2016). Although we did not analyze the zonal wind structures in our sensitivity simulation suite, we infer from the previous comparisons that these features are robust and strongly imply that for each orbital configuration there is a Goldilocks—a fairy tale where Goldilocks finds the perfect combination of chair size, food temperature, and mattress firmness to satisfy her—combination of orbit and ice sheets.

5 Conclusions

An ongoing issue with studying the Paleoclimate is the lack of high resolution spatial and temporal proxy datasets to compare with simulations. Thus, current state-of-the-art simulations use linear regressions to combine all these effects into a range of variances before comparing that with the available proxy data. However, our analysis shows that there are substantial differences between ice sheet configurations that develop as non-linear interactions with orbital changes. This is a critical insight, as the primary paleo modeling intercomparison projects are focused on capturing different states utilizing only one model configuration (Morrill et al., 2013; Ivanovic et al., 2016), whereas a battery of sensitivity simulations could potentially resolve proxy-model discrepancies.

There is a clear Clausius-Clayperon relationship between temperature and precipitation. However, our changes to ice sheets and orbit interactions demonstrate a critical role to the structural changes in temperature and precipitation. The weakening of stationary waves over the North Pacific between orbits and a lowered ice sheet height is reflected in the temperature and precipitation fields, and there are subtle regional effects driven by orbit changes that are not always explained by changes in ice sheet height. For example, higher ice sheets induce a global temperature increase, but within specific European regions there are non-linear changes in warming or cooling that are unexplained by ice sheet changes. As the ice sheet height is lowered, the changes in Europe do not change linearly and are dependent on orbit configuration.

Therefore, there are specific pathways as the climate of the Quaternary changes that occur due to ice sheet heights and orbits combining and interacting, implying a theoretical constraint on the real climate state in the past and giving more confidence to our future projections. In a linear system, these 16 Quaternary states (represented by each sensitivity test) would represent the variability of the Quaternary, but as this is a non-linear system, only one state is physically possible for a given orbit. As the spatial and temporal resolution of the Quaternary proxy data improves, combined with these modeled climates, we expect substantial constraints on realistic climate states, and our simulation suite and methods may help researchers search for new proxy locations to test this hypothesis.

Code and data availability. Tierney et al. (2020b) reanalysis data is available from https://doi.org/10.1594/PANGAEA.920596. Rayner et al. (2003) HadSST reanalysis data is available from https://www.metoffice.com. Code and data for simulations used in this manuscript is available from Buzan et al. (2023).

https://doi.org/10.5194/egusphere-2023-324
Preprint. Discussion started: 6 March 2023

Author contributions. JRB wrote the manuscript, designed the Quaternary and Preindustrial experiments, and executed the simulations. ER contributed to experimental design. WMK executed the Late Holocene and RCP8.5 simulations. CCR contributed to the manuscript and guided the project as principle investigator. All authors contributed to the final version of the manuscript.

Competing interests. The authors declare no competing interests.

Acknowledgements. The authors thanks Brittany Claytor for her edits. This project was funded by NAGRA. The simulations were performed on the super computing architecture of the Swiss National Supercomputing Centre (CSCS). CCR received additional support by the Schweizerischer Nationalfonds zur Förderung der Wissenschaftlichen Forschung (grant no. 200021-162444).

https://doi.org/10.5194/egusphere-2023-324
Preprint. Discussion started: 6 March 2023

References

Abe-Ouchi, A., Saito, F., Kageyama, M., Braconnot, P., Harrison, S. P., Lambeck, K., Otto-Bliesner, B. L., Peltier, W. R., Tarasov, L., Peterschmitt, J.-Y., and Takahashi, K.: Ice-sheet configuration in the CMIP5/PMIP3 Last Glacial Maximum experiments, Geoscientific Model Development, 8, 3621–3637, https://doi.org/10.5194/gmd-8-3621-2015, 2015.

Acosta, R. P., Ladant, J.-B., Zhu, J., and Poulsen, C. J.: Evolution of the Atlantic Intertropical Convergence Zone, and the South American and African Monsoons over the past 95-Myr and their impact on the tropical rainforests, Paleoceanography and Paleoclimatology, 37, e2021PA004 383, https://doi.org/https://doi.org/10.1029/2021PA004383, e2021PA004383 2021PA004383, 2022.

Agard, V. and Emanuel, K.: Clausius–Clapeyron scaling of peak CAPE in continental convective storm environments, Journal of the Atmospheric Sciences, 74, 3043 – 3054, https://doi.org/10.1175/JAS-D-16-0352.1, 2017.

Annan, J. D. and Hargreaves, J. C.: A new global reconstruction of temperature changes at the Last Glacial Maximum, Climate of the Past, 9, 367–376, 2013.

Annan, J. D., Hargreaves, J. C., and Mauritsen, T.: A new global surface temperature reconstruction for the Last Glacial Maximum, Climate of the Past, 18, 1883–1896, https://doi.org/10.5194/cp-18-1883-2022, 2022.

Bartlein, P. J., Harrison, S. P., Brewer, S., Connor, S., Davis, B. A. S., Gajewski, K., Guiot, J., Harrison-Prentice, T. I., Henderson, A., Peyron, O., Prentice, I. C., Scholze, M., Seppä, H., Shuman, B., Sugita, S., Thompson, R. S., Viau, A. E., Williams, J., and Wu, H.: Pollen-based continental climate reconstructions at 6 and 21 ka: a global synthesis, Climate Dynamics, 37, 775–802, https://doi.org/10.1007/s00382-010-0904-1, 2011.

Batchelor, C. L., Margold, M., Krapp, M., Murton, D. K., Dalton, A. S., Gibbard, P. L., Stokes, C. R., Murton, J. B., and Manica, A.: The configuration of Northern Hemisphere ice sheets through the Quaternary, Nature Communications, 10, 1–10, https://doi.org/10.1038/s41467-019-11601-2, 2019.

Brady, E. C., Otto-Bliesner, B. L., Kay, J. E., and Rosenbloom, N.: Sensitivity to Glacial Forcing in the CCSM4, Journal of Climate, 26, 1901 – 1925, https://doi.org/10.1175/JCLI-D-11-00416.1, 2013.

Brandefelt, J. and Otto-Bliesner, B. L.: Equilibration and variability in a Last Glacial Maximum climate simulation with CCSM3, Geophysical Research Letters, 36, https://doi.org/https://doi.org/10.1029/2009GL040364, 2009.

Bryan, K.: Accelerating the Convergence to Equilibrium of Ocean-Climate Models, Journal of Physical Oceanography, 14, 666 – 673, https://doi.org/10.1175/1520-0485(1984)014<0666:ATCTEO>2.0.CO;2, 1984.

Buzan, J. R., Russo, E., Kim, W. M., and Raible, C.: Code and Data for Winter sensitivity of glacial states to orbits and ice sheet heights in CESM1.2, https://doi.org/10.5281/zenodo.7665583, 2023.

Claussen, M., Mysak, L., Weaver, A., Crucifix, M., Fichefet, T., Loutre, M.-F., Weber, S., Alcamo, J., Alexeev, V., Berger, A., Calov, R., Ganopolski, A., Goosse, H., Lohmann, G., Lunkeit, F., Mokhov, I., Petoukhov, V., Stone, P., and Wang, Z.: Earth system models of intermediate complexity: Closing the gap in the spectrum of climate system models, Climate Dynamics, 18, 579–586, https://doi.org/10.1007/s00382-001-0200-1, 2002.

Cleator, S. F., Harrison, S. P., Nichols, N. K., Prentice, I. C., and Roulstone, I.: A new multivariable benchmark for Last Glacial Maximum climate simulations, Climate of the Past, 16, 699–712, https://doi.org/10.5194/cp-16-699-2020, 2020.

CLIMAP: Seasonal reconstructions of the Earth's surface at the Last Glacial Maximum in map series, Technical Report MC-36, 1981.

Dalton, A. S., Stokes, C. R., and Batchelor, C. L.: Evolution of the Laurentide and Innuitian ice sheets prior to the Last Glacial Maximum (115 ka to 25 ka), Earth-Science Reviews, 224, 103 875, https://doi.org/https://doi.org/10.1016/j.earscirev.2021.103875, 2022.

https://doi.org/10.5194/egusphere-2023-324
Preprint. Discussion started: 6 March 2023

Danabasoglu, G., Bates, S. C., Briegleb, B. P., Jayne, S. R., Jochum, M., Large, W. G., Peacock, S., and Yeager, S. G.: The CCSM4 ocean component, Journal of Climate, 25, 1361–1389, https://doi.org/10.1175/JCLI-D-11-00091.1, 2012.

de Vernal, A., Rosell-Melé, A., Kucera, M., Hillaire-Marcel, C., Eynaud, F., Weinelt, M., Dokken, T., and Kageyama, M.: Comparing proxies for the reconstruction of LGM sea-surface conditions in the northern North Atlantic, Quaternary Science Reviews, 25, 2820–2834, https://doi.org/10.1016/J.QUASCIREV.2006.06.006, 2006.

EPICA Community Members: Eight glacial cycles from an Antarctic ice core EPICA community members*, Nature, 429, 623–628, www.nature.com/nature, 2004.

Evensen, G.: The Ensemble Kalman Filter: Theoretical formulation and practical implementation, Ocean Dynamics, 53, 343–367, https://doi.org/10.1007/s10236-003-0036-9, 2003.

Ganopolski, A. and Brovkin, V.: Simulation of climate, ice sheets and CO_2 evolution during the last four glacial cycles with an Earth system model of intermediate complexity, Climate of the Past, 13, 1695–1716, https://doi.org/10.5194/cp-13-1695-2017, 2017.

Hofer, D., Raible, C. C., Dehnert, A., and Kuhlemann, J.: The impact of different glacial boundary conditions on atmospheric dynamics and precipitation in the North Atlantic region, Climate of the Past, 8, 935–949, https://doi.org/10.5194/cp-8-935-2012, 2012a.

Hofer, D., Raible, C. C., Merz, N., Dehnert, A., and Kuhlemann, J.: Simulated winter circulation types in the North Atlantic and European region for preindustrial and glacial conditions, Geophysical Research Letters, 39, https://doi.org/10.1029/2012GL052296, 2012b.

Holden, P., Edwards, N., and Wolff, E.: Multiple West Antarctic ice sheet retreats could explain southern warmth in recent interglacials, in: IOP Conference Series. Earth and Environmental Science, vol. 6, IOP Publishing, 2009.

Hurrell, J. W., Holland, M. M., Gent, P. R., Ghan, S., Kay, J. E., Kushner, P. J., Lamarque, J.-F., Large, W. G., Lawrence, D., Lindsay, K., Lipscomb, W. H., Long, M. C., Mahowald, N., Marsh, D. R., Neale, R. B., Rasch, P., Vavrus, S., Vertenstein, M., Bader, D., Collins, W. D., Hack, J. J., Kiehl, J., Marshall, S., Hurrell, J. W., Holland, M. M., Gent, P. R., Ghan, S., Kay, J. E., Kushner, P. J., Lamarque, J.-F., Large, W. G., Lawrence, D., Lindsay, K., Lipscomb, W. H., Long, M. C., Mahowald, N., Marsh, D. R., Neale, R. B., Rasch, P., Vavrus, S., Vertenstein, M., Bader, D., Collins, W. D., Hack, J. J., Kiehl, J., and Marshall, S.: The Community Earth System Model: A framework for collaborative research, Bulletin of the American Meteorological Society, 94, 1339–1360, https://doi.org/10.1175/BAMS-D-12-00121.1, 2013.

Ivanovic, R., Gregoire, L., Kageyama, M., Roche, D., Valdes, P., Burke, A., Drummond, R., Peltier, W. R., and Tarasov, L.: Transient climate simulations of the deglaciation 21-9 thousand years before present (version 1)-PMIP4 Core experiment design and boundary conditions, Geoscientific Model Development, 2016.

Kageyama, M., Albani, S., Braconnot, P., Harrison, S. P., Hopcroft, P. O., Ivanovic, R. F., Lambert, F., Marti, O., Peltier, W. R., Peterschmitt, J.-Y., Roche, D. M., Tarasov, L., Zhang, X., Brady, E. C., Haywood, A. M., LeGrande, A. N., Lunt, D. J., Mahowald, N. M., Mikolajewicz, U., Nisancioglu, K. H., Otto-Bliesner, B. L., Renssen, H., Tomas, R. A., Zhang, Q., Abe-Ouchi, A., Bartlein, P. J., Cao, J., Li, Q., Lohmann, G., Ohgaito, R., Shi, X., Volodin, E., Yoshida, K., Zhang, X., and Zheng, W.: The PMIP4 contribution to CMIP6 – Part 4: Scientific objectives and experimental design of the PMIP4-CMIP6 Last Glacial Maximum experiments and PMIP4 sensitivity experiments, Geoscientific Model Development, 10, 4035–4055, https://doi.org/10.5194/gmd-10-4035-2017, 2017.

Kageyama, M., Braconnot, P., Harrison, S. P., Haywood, A. M., Jungclaus, J. H., Otto-Bliesner, B. L., Peterschmitt, J.-Y., Abe-Ouchi, A., Albani, S., Bartlein, P. J., Brierley, C., Crucifix, M., Dolan, A., Fernandez-Donado, L., Fischer, H., Hopcroft, P. O., Ivanovic, R. F., Lambert, F., Lunt, D. J., Mahowald, N. M., Peltier, W. R., Phipps, S. J., Roche, D. M., Schmidt, G. A., Tarasov, L., Valdes, P. J., Zhang, Q., and Zhou, T.: The PMIP4 contribution to CMIP6 – Part 1: Overview and over-arching analysis plan, Geoscientific Model Development, 11, 1033–1057, https://doi.org/10.5194/gmd-11-1033-2018, 2018.

https://doi.org/10.5194/egusphere-2023-324
Preprint. Discussion started: 6 March 2023

Lambert, F., Delmonte, B., Petit, J. R., Bigler, M., Kaufmann, P. R., Hutterli, M. A., Stocker, T. F., Ruth, U., Steffensen, J. P., and Maggi, V.: Dust-climate couplings over the past 800,000 years from the EPICA Dome C ice core, Nature, 452, 616–619, https://doi.org/10.1038/nature06763, 2008.

Liakka, J. and Löfverström, M.: Arctic warming induced by the Laurentide Ice Sheet topography, Climate of the Past, 14, 887–900, https://doi.org/10.5194/cp-14-887-2018, 2018.

Liakka, J., Löfverström, M., and Colleoni, F.: The impact of the North American glacial topography on the evolution of the Eurasian ice sheet over the last glacial cycle, Climate of the Past, 12, 1225–1241, https://doi.org/10.5194/cp-12-1225-2016, 2016.

Löfverström, M., Caballero, R., Nilsson, J., and Kleman, J.: Evolution of the large-scale atmospheric circulation in response to changing ice sheets over the last glacial cycle, Climate of the Past, 10, 1453–1471, https://doi.org/10.5194/cp-10-1453-2014, 2014.

Löfverström, M., Caballero, R., Nilsson, J., and Messori, G.: Stationary wave reflection as a mechanism for zonalizing the Atlantic winter jet at the LGM, Journal of the Atmospheric Sciences, 73, 3329 – 3342, https://doi.org/10.1175/JAS-D-15-0295.1, 2016.

Meehl, G. A., Washington, W. M., Arblaster, J. M., Hu, A., Teng, H., Kay, J. E., Gettelman, A., Lawrence, D. M., Sanderson, B. M., and Strand, W. G.: Climate change projections in CESM1(CAM5) compared to CCSM4, Journal of Climate, 26, 6287 – 6308, https://doi.org/10.1175/JCLI-D-12-00572.1, 2013.

Merz, N., Raible, C. C., Fischer, H., Varma, V., Prange, M., and Stocker, T. F.: Greenland accumulation and its connection to the large-scale atmospheric circulation in ERA-Interim and paleoclimate simulations, Climate of the Past, 9, 2433–2450, https://doi.org/10.5194/cp-9-2433-2013, 2013.

Merz, N., Born, A., Raible, C. C., Fischer, H., and Stocker, T. F.: Dependence of Eemian Greenland temperature reconstructions on the ice sheet topography, Climate of the Past, 10, 1221–1238, https://doi.org/10.5194/cp-10-1221-2014, 2014a.

Merz, N., Gfeller, G., Born, A., Raible, C. C., Stocker, T. F., and Fischer, H.: Influence of ice sheet topography on Greenland precipitation during the Eemian interglacial, Journal of Geophysical Research: Atmospheres, 119, 10,749–10,768, https://doi.org/10.1002/2014JD021940, 2014b.

Merz, N., Raible, C. C., and Woollings, T.: North Atlantic eddy-driven jet in interglacial and glacial winter climates, Journal of Climate, 28, 3977–3997, https://doi.org/10.1175/JCLI-D-14-00525.1, 2015.

Merz, N., Born, A., Raible, C. C., and Stocker, T. F.: Warm Greenland during the last interglacial: The role of regional changes in sea ice cover, Climate of the Past, 12, 2011–2031, https://doi.org/10.5194/cp-12-2011-2016, 2016.

Morrill, C., Anderson, D. M., Bauer, B. A., Buckner, R., Gille, E. P., Gross, W. S., Hartman, M., and Shah, A.: Proxy benchmarks for intercomparison of 8.2 ka simulations, Climate of the Past, 9, 423–432, https://doi.org/10.5194/cp-9-423-2013, 2013.

Otto-Bliesner, B. L., Rosenbloom, N., Stone, E. J., McKay, N. P., Lunt, D. J., Brady, E. C., and Overpeck, J. T.: How warm was the last interglacial? New model-data comparisons, Philosophical Transactions of the Royal Society A: Mathematical, Physical and Engineering Sciences, 371, 20130 097–20130 097, https://doi.org/10.1098/rsta.2013.0097, 2013.

Otto-Bliesner, B. L., Braconnot, P., Harrison, S. P., Lunt, D. J., Abe-Ouchi, A., Albani, S., Bartlein, P. J., Capron, E., Carlson, A. E., Dutton, A., Fischer, H., Goelzer, H., Govin, A., Haywood, A., Joos, F., LeGrande, A. N., Lipscomb, W. H., Lohmann, G., Mahowald, N., Nehrbass-Ahles, C., Pausata, F. S. R., Peterschmitt, J.-Y., Phipps, S. J., Renssen, H., and Zhang, Q.: The PMIP4 contribution to CMIP6 – Part 2: Two interglacials, scientific objective and experimental design for Holocene and Last Interglacial simulations, Geoscientific Model Development, 10, 3979–4003, https://doi.org/10.5194/gmd-10-3979-2017, 2017.

Peltier, W.: Global Glacial Isostasy and the Surface of the Ice-Age Earth: The ICE-5G (VM2) Model and GRACE, Annual Review of Earth and Planetary Sciences, 32, 111–149, https://doi.org/10.1146/annurev.earth.32.082503.144359, 2004.

https://doi.org/10.5194/egusphere-2023-324
Preprint. Discussion started: 6 March 2023

Peltier, W. R., Argus, D. F., and Drummond, R.: Space geodesy constrains ice age terminal deglaciation: The global ICE-6G_C (VM5a) model, Journal of Geophysical Research: Solid Earth, 120, 450–487, https://doi.org/10.1002/2014JB011176, 2015.

Raible, C. and Blender, R.: Northern Hemisphere midlatitude cyclone variability in GCM simulations with different ocean representations, Climate Dynamics, 22, 239–248, https://doi.org/10.1007/s00382-003-0380-y, 2004.

Rayner, N. A., Parker, D. E., Horton, E. B., Folland, C. K., Alexander, L. V., Rowell, D. P., Kent, E. C., and Kaplan, A.: Global analyses of sea surface temperature, sea ice, and night marine air temperature since the late nineteenth century, Journal of Geophysical Research: Atmospheres, 108, https://doi.org/https://doi.org/10.1029/2002JD002670, 2003.

Schneider von Deimling, T., Ganopolski, A., Held, H., and Rahmstorf, S.: How cold was the last glacial maximum?, Geophysical Research Letters, 33, 2006.

Shin, S.-I., Liu, Z., Otto-Bliesner, B., Brady, E., Kutzbach, J., and Harrison, S.: A simulation of the Last Glacial Maximum climate using the NCAR-CCSM, Climate Dynamics, 20, 127–151, https://doi.org/10.1007/s00382-002-0260-x, 2003.

Stocker, T., Qin, D., Plattner, G.-K., Tignor, M., Allen, S., Boschung, J., Nauels, A., Xia, Y., V., B., and Midgley, P. M. e.: IPCC, 2013 Summary for Policymakers. In: Climate Change 2013: The Physical Science Basis., 2013.

Stocker, T. F., Mysak, L. A., Wright, D. G., Stocker, T. F., Mysak, L. A., and Wright, D. G.: A zonally averaged, coupled ocean-atmosphere model for paleoclimate studies, Journal of Climate, 5, 773–797, https://doi.org/10.1175/1520-0442(1992)005<0773:AZACOA>2.0.CO;2, 1992.

Tierney, J. E., Poulsen, C. J., Montañez, I. P., Bhattacharya, T., Feng, R., Ford, H. L., Hönisch, B., Inglis, G. N., Petersen, S. V., Sagoo, N., Tabor, C. R., Thirumalai, K., Zhu, J., Burls, N. J., Foster, G. L., Goddéris, Y., Huber, B. T., Ivany, L. C., Turner, S. K., Lunt, D. J., McElwain, J. C., Mills, B. J. W., Otto-Bliesner, B. L., Ridgwell, A., and Zhang, Y. G.: Past climates inform our future, Science, 370, https://doi.org/10.1126/science.aay3701, 2020a.

Tierney, J. E., Zhu, J., King, J., Malevich, S. B., Hakim, G. J., and Poulsen, C. J.: Glacial cooling and climate sensitivity revisited, Nature, 584, 569+, https://doi.org/10.1038/s41586-020-2617-x, 2020b.

Timmermann, A., Yun, K.-S., Raia, P., Ruan, J., Mondanaro, A., Zeller, E., Zollikofer, C., Ponce de León, M., Lemmon, D., Willeit, M., and Ganopolski, A.: Climate effects on archaic human habitats and species successions, Nature, 604, 495–501, https://doi.org/10.1038/s41586-022-04600-9, 2022.

Waelbroeck, C., Paul, A., Kucera, M., Rosell-Melé, A., Weinelt, M., Schneider, R., Mix, A. C., Abelmann, A., Armand, L., Bard, E., Barker, S., Barrows, T. T., Benway, H., Cacho, I., Chen, M. T., Cortijo, E., Crosta, X., de Vernal, A., Dokken, T., Duprat, J., Elderfield, H., Eynaud, F., Gersonde, R., Hayes, A., Henry, M., Hillaire-Marcel, C., Huang, C. C., Jansen, E., Juggins, S., Kallel, N., Kiefer, T., Kienast, M., Labeyrie, L., Leclaire, H., Londeix, L., Mangin, S., Matthiessen, J., Marret, F., Meland, M., Morey, A. E., Mulitza, S., Pflaumann, U., Pisias, N. G., Radi, T., Rochon, A., Rohling, E. J., Sbaffi, L., Schäfer-Neth, C., Solignac, S., Spero, H., Tachikawa, K., Turon, J. L., and Members, M. P.: Constraints on the magnitude and patterns of ocean cooling at the Last Glacial Maximum, Nature Geoscience, 2, 127–132, https://doi.org/10.1038/ngeo411, 2009.

Willeit, M., Ganopolski, A., Robinson, A., and Edwards, N. R.: The Earth system model CLIMBER-X v1.0 – Part 1: Climate model description and validation, Geoscientific Model Development, 15, 5905–5948, https://doi.org/10.5194/gmd-15-5905-2022, 2022.

Williams, C. J. R., Guarino, M.-V., Capron, E., Malmierca-Vallet, I., Singarayer, J. S., Sime, L. C., Lunt, D. J., and Valdes, P. J.: CMIP6/PMIP4 simulations of the mid-Holocene and Last Interglacial using HadGEM3: Comparison to me pre-industrial era, previous model versions aim Proxy data, Atmospheric Chemistry and Physics, 16, 1429–1450, https://doi.org/10.5194/cp-16-1429-2020, 2020.

https://doi.org/10.5194/egusphere-2023-324
Preprint. Discussion started: 6 March 2023

Windler, G., Tierney, J. E., Zhu, J., and Poulsen, C. J.: Unraveling glacial hydroclimate in the Indo-Pacific warm pool: Perspectives from water isotopes, Paleoceanography and Paleoclimatology, 35, e2020PA003 985, https://doi.org/https://doi.org/10.1029/2020PA003985, e2020PA003985 2020PA003985, 2020.

Zhu, J., Liu, Z., Brady, E., Otto-Bliesner, B., Zhang, J., Noone, D., Tomas, R., Nusbaumer, J., Wong, T., Jahn, A., and Tabor, C.: Reduced ENSO variability at the LGM revealed by an isotope-enabled Earth system model, Geophysical Research Letters, 44, 6984–6992, https://doi.org/10.1002/2017GL073406, 2017.

Zhu, J., Otto-Bliesner, B. L., Brady, E. C., Poulsen, C. J., Tierney, J. E., Lofverstrom, M., and DiNezio, P.: Assessment of equilibrium climate sensitivity of the Community Earth System Model Version 2 through simulation of the Last Glacial Maximum, Geophysical Research Letters, 48, e2020GL091 220, https://doi.org/https://doi.org/10.1029/2020GL091220, e2020GL091220 2020GL091220, 2021.

Zhu, J., Otto-Bliesner, B. L., Brady, E. C., Gettelman, A., Bacmeister, J. T., Neale, R. B., Poulsen, C. J., Shaw, J. K., McGraw, Z. S., and Kay, J. E.: LGM paleoclimate constraints inform cloud parameterizations and equilibrium climate sensitivity in CESM2, Journal of Advances in Modeling Earth Systems, 14, e2021MS002 776, https://doi.org/https://doi.org/10.1029/2021MS002776, e2021MS002776 2021MS002776, 2022.